Field Precision LLC

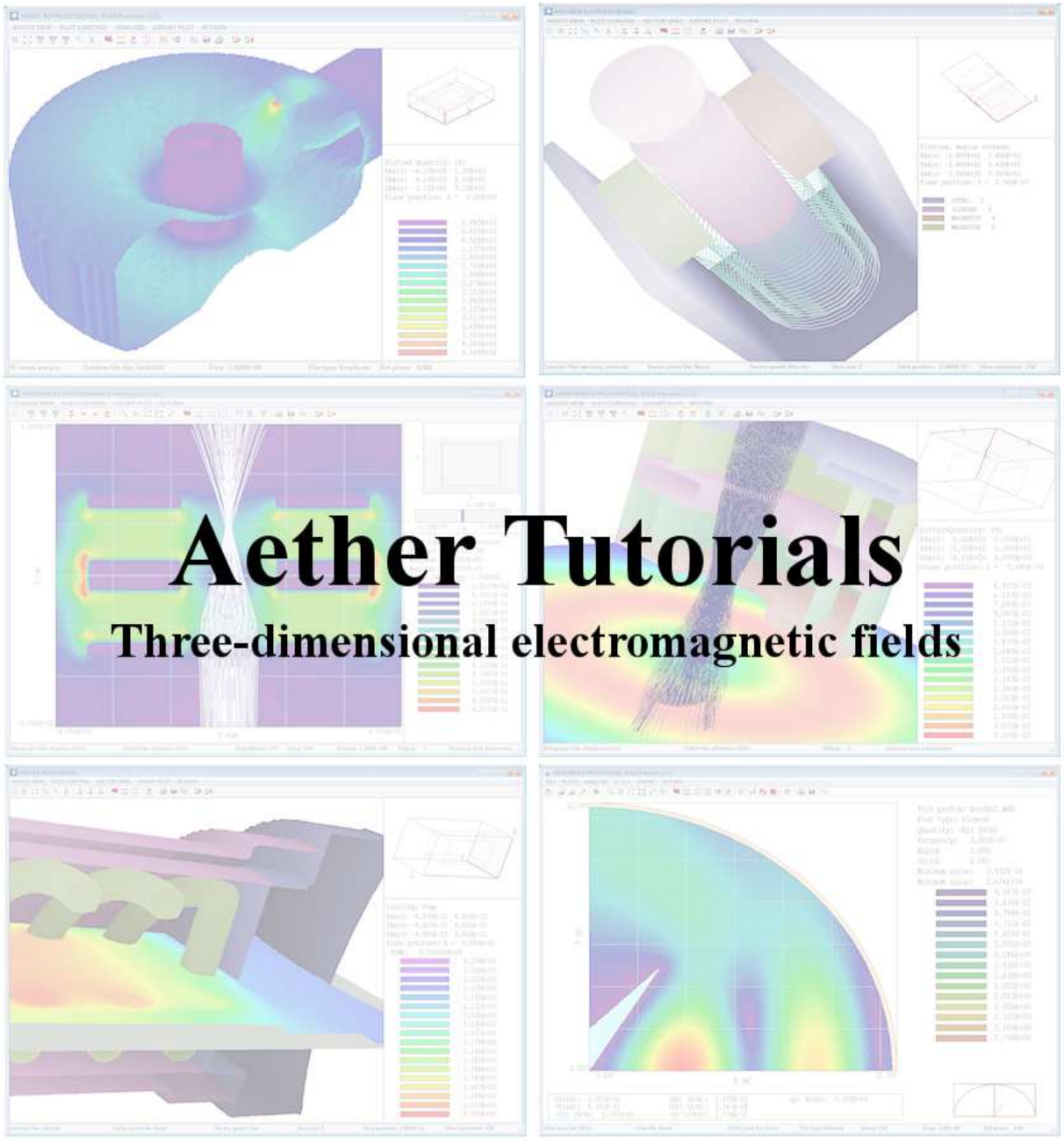

Aether Tutorials

Three-dimensional electromagnetic fields

EMail: techinfo@fieldp.com

URL: http://www.fieldp.com

Contents

1 One-dimensional pulse propagation **3**
- 1.1 Setting up the mesh . . . 3
- 1.2 Propagation in vacuum . . . 4
- 1.3 Reflection from a dielectric boundary . . . 6
- 1.4 Propagation into a graded dielectric . . . 7

2 Driving coaxial transmission lines **9**
- 2.1 Pulse mode solution . . . 10
- 2.2 RF mode solution . . . 11

3 Locating cavity resonant frequencies **14**

4 Calculating fields in a high-Q resonator **18**

5 Resistive load for a pulsed-power system **21**

6 Radiation from a simple dipole **26**

7 Switching transmission lines and capacitors **31**

8 Initial electric-field distributions from HiPhi **35**

9 TE10 mode in a rectangular waveguide **40**

10 TE11 mode in a circular waveguide **45**

11 S matrix for a two-terminal network **48**

12 Half-wave dipole antenna **52**

13 Loaded klystron output cavity **55**
- 13.1 Resonant frequency calculation . . . 55
- 13.2 Mode field calculation . . . 58

14 RF models of a cavity magnetron **60**

1 One-dimensional pulse propagation

To introduce **Aether** techniques and setup procedures, we shall start with *Pulse* mode calculations in the simplest possible geometry – plane electromagnetic pulses with infinite transverse extent. We can make comparisons to theory to get sense of the code's numerical accuracy. Despite their relative simplicity, the examples illustrate several features of *Pulse* mode simulations:

- Defining pulse shapes from tables, mathematical expressions and standard functions.
- Interpreting tables as singular or periodic functions.
- Specifying absorbing boundaries and drive currents.
- Using symmetry boundaries.
- Defining continuous spatial variations of material properties.

1.1 Setting up the mesh

The geometry for all examples is defined by the file `onedim.min`. The system extends from $z_{min} = -100.0$ cm to $z_{max} = 100.0$ cm along the direction of pulse propagation. The element length is $\Delta z = 0.5$ cm. Symmetry boundaries along x and y are used to represent infinite space. The condition means that values of **H** on the boundaries are equal to those on adjacent internal nodes. Therefore, there should be at least one internal node in the x-y plane. the transverse dimensions are set to ± 5.0 cm in x and y with element size $\Delta x = \Delta y = 2.5$ cm to create good plots in **Aerial**.

The solution volume includes five regions:

- The propagation volume is divided into two main parts so we can assign different physical properties. Region *Medium1* initially covers the span $z = -100.0$ cm to $z = 0.0$ cm. The lower part of this region is over-written by regions *Absorb1* and *Source*.
- Region *Medium2* extends from $z = 0.0$ cm to $z = 100$ cm. The upper part is over-written by region *Absorb2*.
- *Absorb1* and *Absorb2* are absorbing layers of thickness $\Delta z = 0.5$ cm at the ends of the solution volume.
- Region **Source** is slab of thickness $\Delta z = 0.5$ cm with the properties of *Medium1* adjacent to *Absorb1*. The slab carries a uniform current density j_y to excite the pulse.

In summary, the order regions along the direction of propagation is *Absorb1*, *Source*, *Medium1*, *Medium2* and *Absorb2*.

A final geometry topic is the motivation for picking the element size along z. The pulse has temporal width 0.66 ns. In vacuum, the spatial width is about 20 cm. Therefore, the

Table 1: Contents of the file `onedim01.ain`

```
* ---- CONTROL ----
Mode = Pulse
Mesh = OneDim
DUnit =  100.0
TMax =  15.0E-9
Dt = 0.010E-9
SymBound XDn
SymBound XUp
SymBound YDn
SymBound YUp
* ---- CURRENT SOURCES ----
SMod(1) = gaussnorm.mod 0.40E-9 1.0
* ---- REGION PROPERTIES ----
Epsi(1) =  1.0
Mu(1) =  1.0
Epsi(2) =  1.0
Mu(2) =  1.0
Epsi(3) =  1.0
Mu(3) =  1.0
Jy(3,1) = 10.0
AbsLayer(4) 0.5
AbsLayer(5) 0.5
* ---- DIAGNOSTICS ----
History =   0.0 0.0 -75.0
History =   0.0 0.0 75.0
EndFile
```

element width $\Delta z = 0.5$ cm gives about 40 elements over the pulse. This number is sufficient for good resolution and moderate numerical dispersion. To follow the example, use **MetaMesh** to process the script, creating the mesh file `onedim.mdf`.

1.2 Propagation in vacuum

The first calculation addresses pulse propagation in a uniform vacuum volume. Table 1 lists the contents of the control script `onedim01.ain`. In the *Control* section, the *Mode* command specifies a time-domain solution. The program obtains the geometry from `onedim.mdf`, where coordinates are given in units of centimeters. The simulation time t_{max} equals the 2.25 times the electromagnetic transit time along the system. The specified time step $\Delta t = 1.0 \times 10^{-9}$ is about 40% below the Courant time step limit. The *SymBound* commands state that there is no variation of **H** normal to the upper and lower boundaries in x and y.

In the *Source* section, the *SMod* command defines a modulation function $m(t)$ as a Gaussian pulse using a table of values in the file `gaussnorm.mod`. Figure 1, a plot of the data points, illustrates a good table well suited to cubic spline interpolations. The points define a smooth curve with continuous values and first derivative. In the default *Single* mode, the modulation

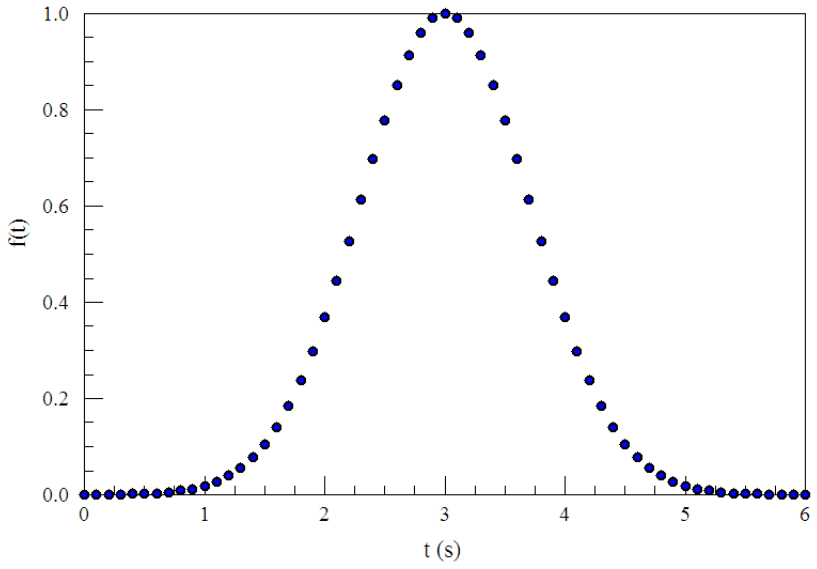

Figure 1: Data points in the file `gaussnorm.mod`.

function is interpreted to have value 0.0 at times $t > 6.0$ s. When loaded into the program, time values are multiplied by 0.4×10^{-9}, giving a pulse with peak at 1.2 ns and full width (at half maximum) of 0.66 ns. The regions *Medium1*(1), *Medium2*(2) and *Source*(3) have the properties of vacuum ($\epsilon_r = 1.0, \mu_r = 1.0$). The region *Source* carries a uniform current density $j_y = 10.0 \times m(t)$ A/m^2. In response to the *AbsLayer* command, **Aether** calculates the conductivity required for a perfect absorber of thickness 0.5 cm. Finally, in the commands of the *Diagnostics* section place monitors 1.5 m apart at $z = \pm 75$ cm.

The **Aether** run creates two probe files. Loading `onedim01.p01` (at $z = -75$ cm) into the **Probe** program and changing the plot quantity to H_x gives the plot of Fig. 2. To find the theoretical peak value of H_x, we multiply the peak source current density by the layer thickness to find a peak linear current density $J_y = 0.05$ A/m. The current is shared equal between the upstream absorber and the propagation volume, so the expected of magnetic field is $H_x = 0.02500$ A/m. The code results in $H_x = 0.2495$ A/m. Changing the plot quantity to E_y, Probe shows a peak value of -9.401 V/m. The theoretical prediction is $377.3 \times H_x = -9.433$ V/m. A comparison of signals in the two probe files shows a time delay of 5.000 ns, close to the predicted electromagnetic transit time of 5.004 ns over the 1.5 m distance. Note that small late-time feature in the trace of Fig. 2 caused by reflection from the downstream absorbing boundary. The reflected power is only 0.01% of the incident power.

The following alternate forms of the SMod command will give identical results:

```
SMod(1) = gaussian 1.2E-9 0.66E-9
SMod(1) > exp(-0.69315*(($t-1.2E-9)/0.33E-9)^2)
```

This form gives a periodic train of Gaussian pulses with a separation of 2.4 ns:

```
SMod(1) = gaussnorm.mod periodic 0.40E-9 1.0
```

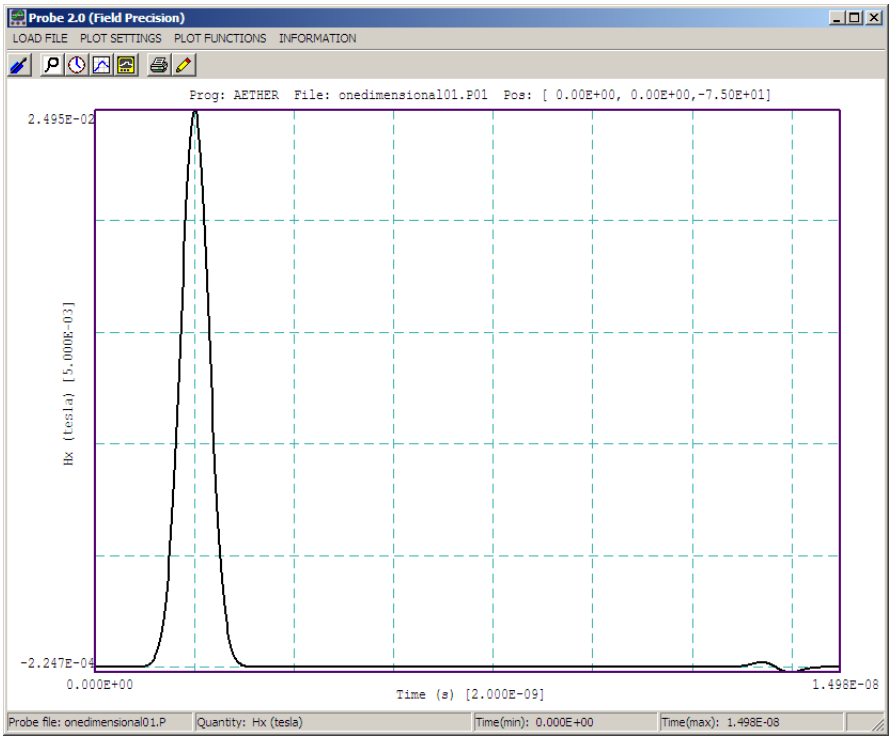

Figure 2: Plot of $H_x(t)$ at $z = -75.0$ cm created by **Probe**.

1.3 Reflection from a dielectric boundary

This next calculation models pulse reflection from a dielectric boundary. The geometry is the same as the previous calculation. The difference is that a relative dielectric constant $epsilon_r = 5.0$ is assigned to *Medium2*. In comparison to the file `onedim01.ain` in Table 1, the file `onedim02.ain` includes the following lines:

```
Epsi(2) =  5.0
AbsLayer(5) 0.5 5.0 1.0
```

The additional parameters in the *AbsLayer* command for region *Absorb2* signal that **Aether** should match the impedance of the adjacent material. The vacuum region has characteristic impedance $\eta_1 = 377.3\ \Omega$ while *Medium2* has $\eta_1 = 168.7\ \Omega$. Inspection of the listing file shows that **Aether** has assigned the conductivity $\sigma = 1/\eta_2 \Delta z = 1.186$ S/m.

Figure 3 is a plot of $E_x(t)$ for a probe in the vacuum region at $z = -75.0$ cm. As expected, the incident and reflected peaks are separated by an interval of 5.0 ns. If the incident pulse has peak electric-field amplitude E_0, then the prediction for the reflected pulse amplitude is

$$E_r = E_0 \, \frac{\eta_2 - \eta_1}{\eta_2 + \eta_1} = -0.382. \tag{1}$$

The code result is $E_r/E_0 = -0.383$. Again, the effectiveness of upstream and downstream boundaries in absorbing the reflected and transmitted pulses is evident in the long-term plot.

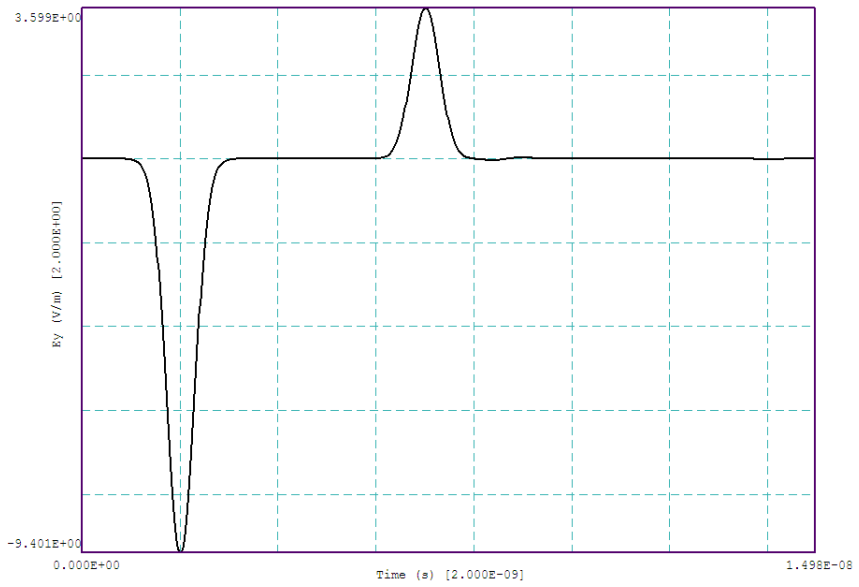

Figure 3: Incident and reflected pulses -75 cm upstream from a dielectric boundary between vacuum and a medium with $\epsilon_r = 5.0$.

1.4 Propagation into a graded dielectric

The final example is a one-dimensional calculation that would be difficult to approach with analytic methods. A pulse is incident on a graded dielectric. The relative dielectric constant changes smoothly from $\epsilon_r = 1.0$ to $\epsilon_r = 5.0$ over the length of *Medium2*. The file `onedim03.ain` contains one line that differs from the previous example script:

```
Epsi(2) > 1.0 + 2.0*(1.0 - COS(0.031416*$z))
```

The line illustrates the use of an algebraic expression to assign a spatial variation of material properties over a region. The top plot in Fig. 4 shows a slice plot of $\epsilon_r(z, x)$ created in **Aerial**. The middle plots show $H_x(z, x)$ at times $t = 4.0$ ns and 7.0 ns. Notice how the spatial length of the pulse shortens in the dielectric medium. The lower part of Fig. 4 plots $H_x(t)$ at the probe position in the vacuum region ($z = -75.0$ cm). Compared to the previous example, the reflected pulse has reduced amplitude but an increased extent in time.

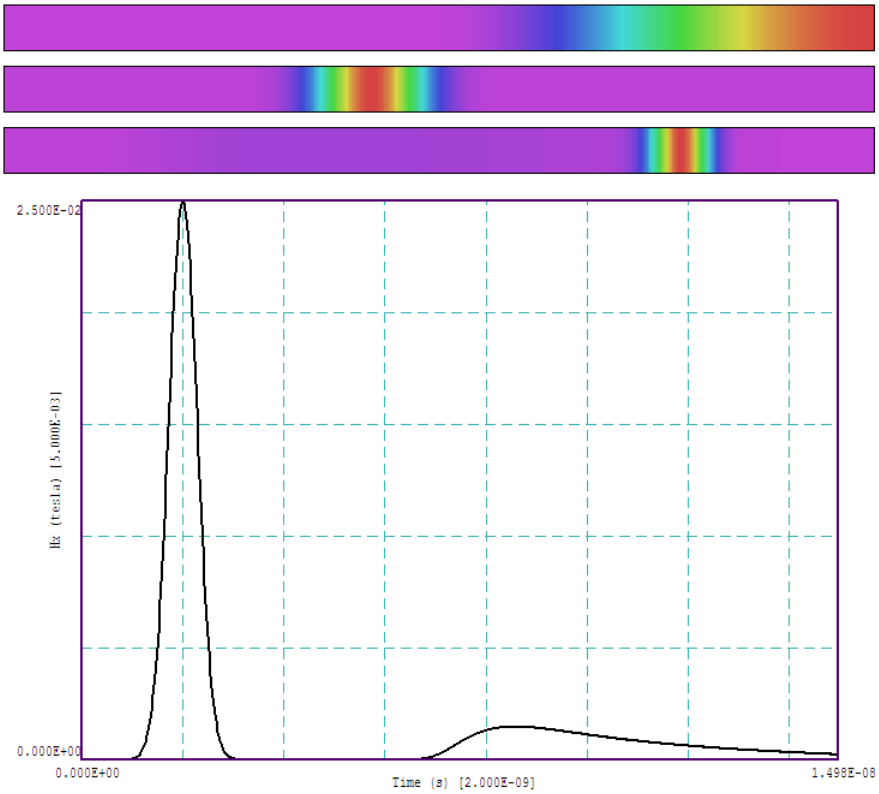

Figure 4: Reflection from a graded dielectric region. Top: spatial variation of ϵ_r (violet: 1.0, red: 5.0). Middle: spatial variation of $H_x(z)$ at early and late times. Bottom: temporal variation of $H_x(t)$ at $z = -75.0$ cm.

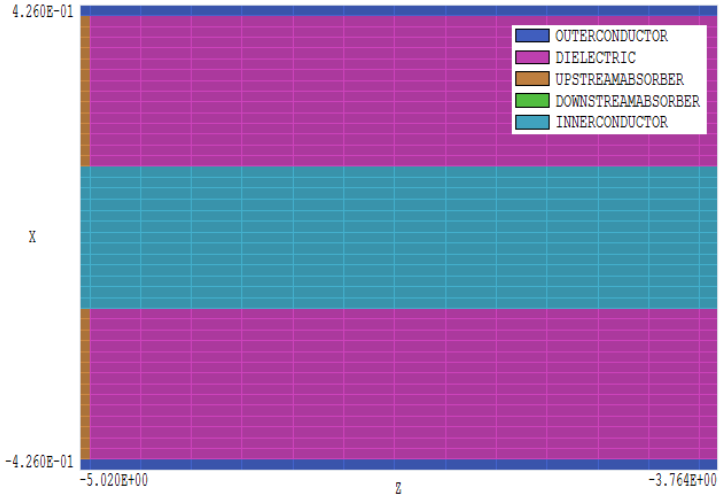

Figure 5: Geometry for the TLINE50 example, detail of the source end of the transmission line, view in the plane $y = 0.0$ cm.

2 Driving coaxial transmission lines

Coaxial transmission lines are often used to drive antennas and other microwave devices. The examples covered in this chapter show how to generate TEM pulses and waves in a 50Ω coaxial cable. They also, give an opportunity to review some transmission line theory and check validity and accuracy of the code. The following section addresses time-domain pulsed solutions, while Sect. ssect:coaxrf concentrates on wave propagation.

The file `TLINE50.MIN` defines the geometry for both calculations. The mesh represents a 10 cm length of cable with outer radius $r_o = 0.406$ cm and inner radius $r_i = 0.130$ cm. The element length in the x-y plane is 0.02 cm. The element length along z is 0.1 cm except for the absorbing layers which have thickness 0.02 cm. The motivation for the choice is that the performance of absorbers improves with decreasing thickness. The is no penalty in the run time because the Courant time step is based on the minimum element dimension in any direction. The following forms of the *XMesh* and *YMesh* structures ensure that elements have boundaries close to those of the solution-volume regions:

```
XMesh
  -0.426 -0.406 N  1
  -0.406 -0.130 N 14
  -0.130  0.130 N 13
   0.130  0.406 N 14
   0.406  0.426 N  1
End
```

The mesh construction strategy has three steps:

- Fill the entire solution volume with the outer conductor region.

- Carve out cylindrical regions to represent the line medium and the absorbers at the two ends.
- Add the center-conductor region.

Aether is an element-based code and does not use region-number information at nodes. In contrast to **HiPhi**, it is not necessary to worry about the order of dielectric and metal regions in the mesh file or to use the *Coat* command.

2.1 Pulse mode solution

The dielectric medium of the cable is polyethylene with $\epsilon_r = 1.871$ and $\sigma = 0.0$. The impedance of the medium is $\eta = 275.4\ \Omega$. The line has a characteristic impedance

$$Z_0 = \frac{\eta}{2\pi}\ \ln\left(\frac{r_o}{r_i}\right) = 49.92\ \Omega. \tag{2}$$

Using the setup of Fig. 5, the goal is to generate a square pulse that traverses the line and terminates at the downstream absorber.

We shall consider some features of the script `TLINE50PULSE.AIN`. The single transit time for a pulse in the line is about 0.46 ns, so we choose a maximum simulation time of 1.00 ns to check for reflections. For easy comparisons, we shall launch a pulse with a peak current amplitude of 1.0 A. Because half the drive current is lost as backflow in the upstream absorber, the peak current should be $I = 2.0$ A. The absorber layer has thickness $\Delta z = 0.0002$ m. The current density should flow in the radial direction with amplitude

$$j_r(r) = \frac{I}{2\pi r \Delta z} = \frac{1592.0}{r}\ (\mathrm{A/m^2}). \tag{3}$$

The following statements the spatial variation of current density in the source region:

```
Jx(4,1) > 1592.0*$x/($x^2 + $y^2)
Jy(4,1) > 1592.0*$y/($x^2 + $y^2)
```

The statement

```
SMod(1) = Square 0.05E-9 0.45E-9 0.10E-9
```

sets the time variation of Source 1. The rounded square pulse starts at 0.05 ns and ends at 0.45 ns, with rise and fall times of 0.10 ns. Finally, note that the *AbsLayer* and *Metal* region statements use the long form to show the layers are adjacent to a non-vacuum medium.

To check numerical values, probes are placed at a radius of 0.30 cm ($x = 0.30$ cm, $y = 0.00$ cm) at axial positions $z = -4.95$ cm (source layer), $z = 0.00$ cm (line midpoint) and $z = 4.95$ cm (line end). An inspection of the j_x signal in first probe shows a peak source-layer current density of 1.070×10^5 A/m^2, consistent with Eq. 3. The predicted azimuthal magnetic field of the pulse is given by,

$$H_\theta(r) = \frac{I}{2\pi r}. \tag{4}$$

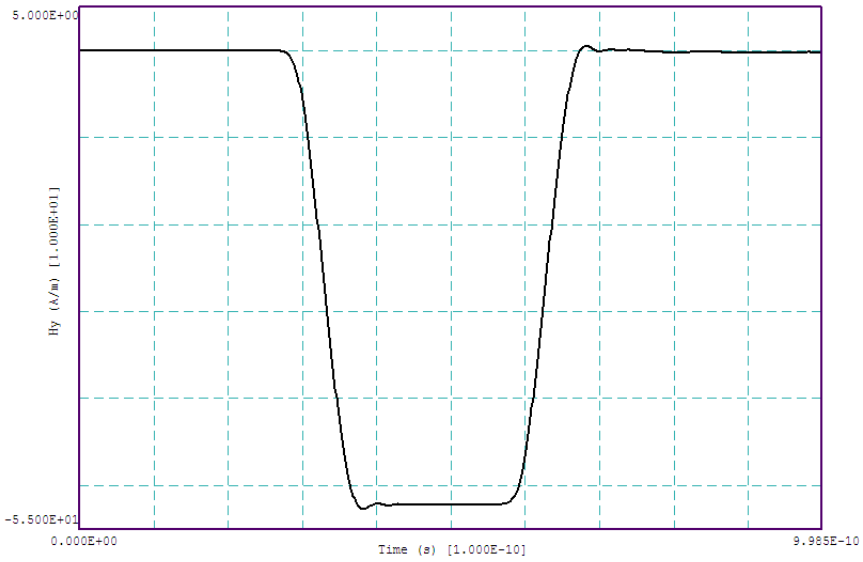

Figure 6: Plot of $H_y(t)$ at $x = 0.3$ cm, $y = 0.0$ cm, $z = 0.0$ cm.

For $I = 1.0$ A and $r = 0.003$ m, the value is $H_\theta = 53.05$ A/m, consistent with the code prediction show in Fig. 6. The figure also illustrates the effectiveness of absorber. The reflected pulse carries less than 0.01% of the incident power. Finally, at $t = 0.25$ ns the volume integrals in Aether and Aerial return the value $p = -48.3$ W for the upstream absorber. The minus sign indicates a net addition of power to the volume. The approximate power balance is the following: 100 W input from the drive current, 50 W lost in the absorber and 50 W transferred to the downstream pulse.

2.2 RF mode solution

In the calculation controlled by `TLINE50RF.AIN`, the source current has amplitude 2.0 A and a harmonic variation at frequency $f = 2.924$ GHz. In the RF mode, the code runs to a steady-state solution and converts the result to a phasor representation. There are only a few differences from the *Pulse* mode script. The *TMax* statement is replaced by

```
Freq = 2.924E9
NPeriod = 5 2
```

The first commands sets the frequency and the second determines the run time. The integers in the *NPeriod* command specify a smooth start of two RF periods followed by steady-state excitation for three RF periods. The smooth start avoids the generation of high frequency noise associated with discontinuous excitation. The steady-state period allows equilibration of waves along the line. **Aether** temporarily records the field values at the end of four periods and then runs for an addition quarter period. The final values are compared to the recorded ones to find the amplitude and phase of field quantities.

There are two commands in the Diagnostics section:

```
History = (0.30, 0.00,  0.00)
Probe = (0.30, 0.00,  4.95)   Ex
```

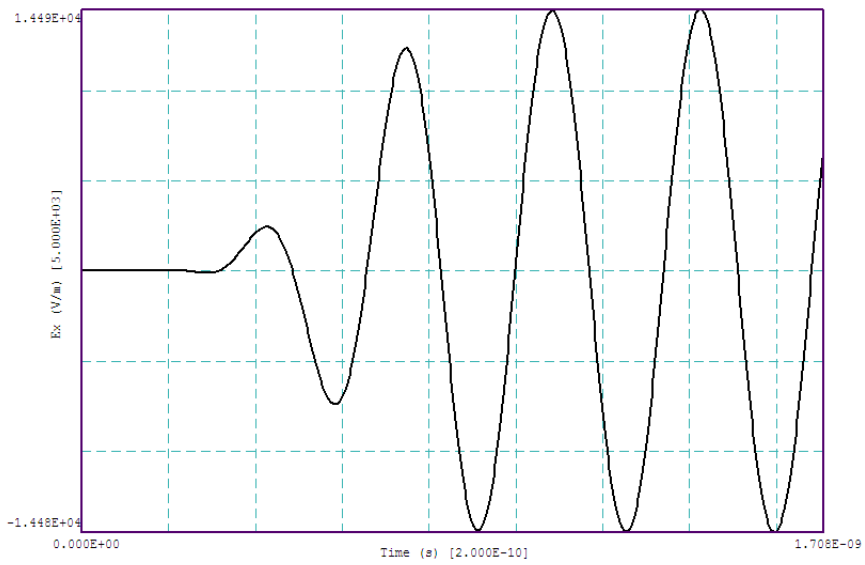

Figure 7: Variation of $E_x(t)$ at position $x = 0.3$ cm, $y = 0.0$ cm, $z = 0.0$ cm, example `TLINE50RF`.

The first command defines a standard monitor where recorded field quantities can be displayed with **Probe**. In response to the *Probe* command, **Aether** checks the value of E_x at the end of the system and records relative changes in the listing file.

Figure 7 shows the evolution of electric field at the midpoint of the line. The data confirm that the solution reaches a steady state with a pure harmonic excitation at 2.924 GHz. Analysis of the output file with **Aerial** shows a spatial variation of field quantities consistent with a traveling wave with $\lambda = 7.5$ cm. In the *Slice plot* menu, we can create a useful display by switching from the *Amplitude* mode and picking the slice plane $y = 0.0$. All quantities appear uniform along z in the propagation medium because an ideal traveling wave has constant amplitude. To detect small variations, set the scan quantity to H_y and take a line scan along z at $x = 0.3$ cm. The quantity varies between 51.99 A/m and 52.49 A/m. This implies a standing-wave ratio (SWR) from which we can derive the reflection coefficient Γ from the downstream resistor. The ratio is defined as

$$S = \frac{|H|_{max}}{|H|_{min}} = \frac{1 + |\Gamma|}{1 - |\Gamma|}, \tag{5}$$

or

$$|\Gamma| = \frac{S - 1}{S + 1}. \tag{6}$$

In this case, $S = 1.010$, giving $|\Gamma| = 4.79 \times 10^{-3}$. For the thin absorbing layer with normal wave incidence, the reflected power ratio is only 2.3×10^{-5}.

To conclude, we can check the integral quantities recorded in the listing file, show in Table 2. The theoretical average power carried by a 1.0 A wave in a 50Ω transmission line is 25 W. The listing shows a net power 24.4146 W added in the upstream absorber and 24.4156 W lost in the downstream absorber. As expected, the electrical and magnetic field energies in the propagation volume (Region 2) are almost identical. For comparison, the time-averaged

Table 2: Energy integrals listed in `TLINE50RF.ALS`.

```
Energy and power volume integrals
Global quantities
   Electric field energy:   5.59864E-09 (J)
   Magnetic field energy:   5.51347E-09 (J)
   Total field energy:   1.11121E-08 (J)
   Resistive power dissipation:   9.01456E-03 (W)
Region quantities
    NReg  ElecEnergy   MagEnergy    TotEnergy      Power
              (J)          (J)          (J)          (W)
   ========================================================
      1  0.00000E+00  0.00000E+00  0.00000E+00  0.00000E+00
      2  5.57644E-09  5.50793E-09  1.10844E-08  0.00000E+00
      3  1.11743E-11  2.74154E-12  1.39159E-11 -2.41467E+01
      4  1.10214E-11  2.80640E-12  1.38278E-11  2.41557E+01
      5  0.00000E+00  0.00000E+00  0.00000E+00  0.00000E+00
```

magnetic field energy in a transmission line is given by $U_m = LI^2/4$, where the inductance for a length D is

$$L = \frac{\mu_0}{2\pi} \ln\left(\frac{r_o}{r_i}\right) D. \tag{7}$$

Inserting values, we find that $L = 2.255 \times 10^{-6}$ H and $U_m = 5.64 \times 10^{-9}$ J.

3 Locating cavity resonant frequencies

A primary function of **Aether** is to locate the resonant frequencies of three-dimensional structures. This section illustrates how to implement the *Res* mode. Once frequencies have been located, you can generate the full field pattern for the resonance using the *RF* mode. As in other tutorials, we shall consider a relatively simple geometry to make comparisons to theory. Nonetheless, the examples cover all techniques and can act as templates for extensions to complex resonators.

The computational strategy in **Aether** is to excite a structure with a pulse whose Fourier transform has a well-defined frequency spectrum and width. The program monitors time-dependent fields at one or more locations. Peaks in the Fourier transform of the probe signals correspond to resonant modes. This method has two advantages over direct searches for eigenfrequencies:

- Calculations take considerably less time and are well matched to personal computers.
- The procedure works for structures with very low values of Q (the quality factor). You can locate resonances in strongly-damped cavities and open systems.

The examples of this chapter treat a cylindrical cavity resonator with radius $R = 15.0$ and length along z of 10.0 cm. The first calculation seeks modes of type TM_{0n0} in an undamped cavity ($Q = \infty$). The fields of the modes are uniform in z and θ. The file `CYLCAVONO.MIN` defines a mesh with an element size of 0.5 cm. The file illustrates how to represent a closed cavity with metal walls. The solution volume extends from -15.5 cm to $+15.5$ cm in x and y and -5.5 cm to $+5.5$ cm in z. To create the metal walls, we first fill the entire solution volume with elements of Region 1. Next, we carve out a cylinder with the cavity dimensions. Elements of Region 2 have the properties of vacuum. Finally, we add a small box (Region 3) with vacuum properties that carries an oscillating current density to excite the modes. The integrated volume of the elements of Regions 2 and 3 is 7070.00 cm^3, while the theoretical value for the cylindrical cavity is 7068.58 cm^3. The values imply that the effective radius of the cavity differs by about 0.1% from the theoretical value, giving a sense of the accuracy limit for determining frequency.

To achieve the best results, it is useful to have a qualitative idea of the mode field variations. Modes of type TM_{0n0} have field components E_z and H_θ. The theoretical values of resonant frequencies are given by:

$$f_{0n0} = \frac{\chi_{0n} c}{2\pi R}, \tag{8}$$

where the quantities χ_{0n} are arguments that give zero values of the Bessel function J_0: $\chi_{01} = 2.4048$, $\chi_{02} = 5.5201$, $\chi_{03} = 8.6537$, $\chi_{04} = 11.79153$ and $\chi_{05} = 14.93091$. On the axis, E_z has a maximum value and $H_\theta = 0.0$ A/m. To excite the modes preferentially, we locate Region 3 at position $x = 0.0$ cm, $y = 0.0$ cm and $z = 0.0$ cm with current density component j_z. The magnetic field is non-zero at the cavity wall. For preferential detection of TM_{0n0} modes, we place a probe at position $x = 14.0$ cm, $y = 0.0$ cm and $z = 0.0$ cm and detect the field component H_y.

Table 3: Contents of the **Aether** script `CYLCAVON0.AIN`.

```
* ---- CONTROL ----
Mode = RES
Mesh = CYLCAVON0
DUnit =  100.0
Freq = (1.5E9, 3.0E9)
Source(3) = 0.0 0.0 1.0
* ---- REGION PROPERTIES ----
Metal(1)
Vacuum(2)
Vacuum(3)
* ---- DIAGNOSTICS ----
History =   0.000  0.000  0.000
History =  14.000  0.000  0.000
Probe = 14.000  0.000  0.000 Hy

EndFile
```

Table 3 lists the full script for the **Aether** calculation. The *Control* command

```
Freq 1.5E9 3.0E9
```

sets a central frequency of 1.5 GHz with an excitation frequency spread of 3.0 GHz. The excitation spectrum therefore extends approximately from 0.0 GHz to 3.0 GHz. The broad band encompasses the TM_{010}, TM_{020} and TM_{030} modes. The command

```
Source 3 0.0 0.0 1.0
```

identifies Region 3 as the source and sets j_z as the only non-zero component of current density. The *Diagnostics* section calls for history records on the axis and at the probe location. There is a single probe with position and field component to detect TM_{0n0} modes.

The calculation takes about 80 seconds. In the *Res* mode, **Aether** creates a file of the Fourier transformed signal at each probe location. For this example there is a single file named `CYLCAVON0.P51`. The transformed files are recorded in a standard format so you can view them with the **Probe** utility program. Figure 8 shows the result. Note that the axis labeled *Time* should be interpreted as *Frequency*. **Aether** also creates the following table in the listing file `CYLCAVON0.ALS`:

```
Probe Number  1  File: CylCav0n0.P51
   Predicted resonance frequencies (Hz)
   Number       F           FWidth    Amplitude
   ============================================
        1  7.619289E+08  1.739804E+07   0.5723
        2  1.759157E+09  1.057429E+07   1.0081
        3  2.753150E+09  1.936289E+07   0.6157
        4  2.780901E+09  2.100438E+07   0.3986
        5  3.074668E+09  1.385277E+07   0.1166
```

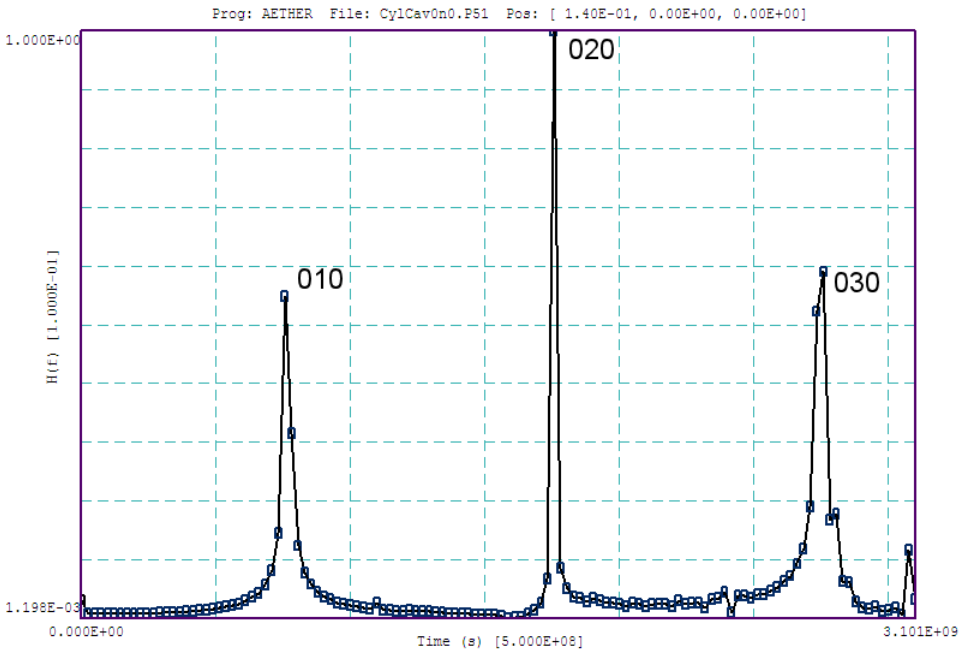

Figure 8: Probe frequency spectrum for TM_{0n0} mode.

Table 4: Computed frequencies of TM_{0n0} modes.

Mode	**f (theo)** (GHz)	**f (code)** (GHz)	**Error** (Percent)
TM_{010}	0.76494	0.76193	-0.393
TM_{020}	1.75588	1.75916	+0.187
TM_{030}	2.75265	2.75315	+0.018

The central frequencies are computed by a peak identification routine. By comparison to Fig. 8, the first three high-amplitude peaks are the TM_{0n0} modes, the fourth peak is glitch in the third resonance and the fifth peak is an undesired mode excited at low level. Table 4 shows a comparison of the code results to theoretical values calculated from Eq. 8.

As the next step, we can modify the calculation to find a more accurate values for the frequency of the TM_{010} mode (`CYLCAV010.AIN`). The file has the following frequency command:

```
Freq  0.80E9 0.40E9
```

There is a narrowed excitation width centered near the frequency determined by the previous calculation. In this case, the frequency listing shows a single peak at 0.76468 GHz, within 0.034% of the theoretical value.

To illustrate how to optimize for different mode types, consider the class TM_{1n0}. These modes are responsible for the *beam breakup instability*, a concern in accelerator physics. Characterizing breakup modes is essential for the design of high-current electron accelerator cavities. The modes have $E_z = 0.0$ on axis with a nonzero $|\mathbf{H}|$. Suppose we excite the cylindrical cavity with a source displaced from the axis along x. In this case, $E_z(0.0, y, z) = 0.0$ and

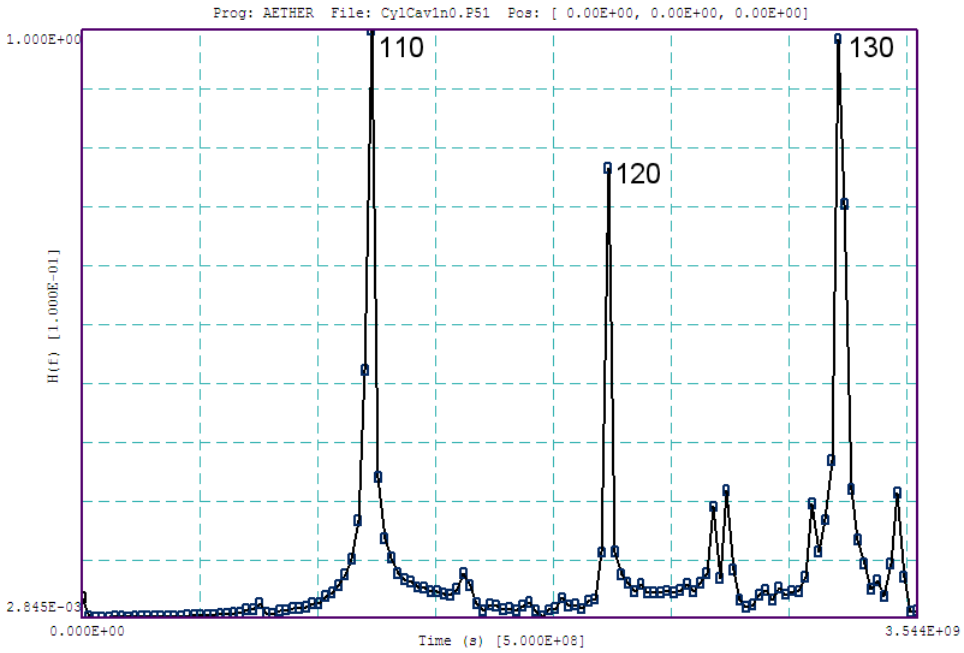

Figure 9: Probe frequency spectrum for TM_{1n0} modes.

$E_z(-x, 0.0, z) = -E_z(x, 0.0, a)$. Accordingly, we construct a modified mesh where Region 3 is displaced a distance $\Delta x = 7.0$ cm (`CYLCAV1N0.MIN`). The first calculation (`CYLCAV1N0.AIN`) is a broadband search for modes. We expect higher mode frequencies, so the central value is shifted to $f_0 = 2.0$ GHz.

The theoretical values of resonant frequency are given by

$$f_{0n0} = \frac{\chi_{1n} c}{2\pi R}, \tag{9}$$

where the quantities χ_{1n} are arguments that give zero values of the Bessel function J_1: $\chi_{11} = 3.832$, $\chi_{12} = 7.016$ and $\chi_{13} = 10.173$. In this case, we locate the probe at the origin and set the detected field component as H_y. Figure 9 shows the probe response. The results of the peak search recorded in the listing file are given in Table 5 along with theoretical values. Again we can narrow the excitation width to find a more accurate frequency value for a specific mode, in this case TM_{110}. The frequency command in the file `CYLCAV110.AIN` is

```
Freq 1.25E9 0.25E9
```

The calculation yields a mode frequency $f_{110} = 1.2190$, within 0.016% of the theoretical value.

Identifying peaks with the *Res* mode is only half the task. There are two outstanding issues:

- How do we know that we have found the right mode?
- What are spatial variations of field quantities required to determine application quantities like the transverse impedance?

Tutorial 4 explains how to use the value of resonant frequency in an RF mode calculation to find the electric and magnetic fields of the TM_{110} mode in a high-Q cavity.

Table 5: Computed frequencies of TM_{1n0} modes.

Mode	**f (theo)** (GHz)	**f (code)** (GHz)	**Error** (Percent)
TM_{110}	1.2188	1.2242	-0.443
TM_{120}	2.2315	2.2343	+0.125
TM_{130}	3.2356	3.2151	+0.634

4 Calculating fields in a high-Q resonator

This tutorial continues the resonant-mode calculation of Tutorial 3. We shall find the electric and magnetic fields for the TM_{110} mode in a cylindrical cavity of radius $R = 15.0$ cm and length $D = 10.0$ cm. The previous calculation yielded a resonant frequency $f = 1.2190$ GHz. The present calculation demonstrates how to drive a mode in a high-Q structure.

The mesh is almost identical to that of Tutorial 3. The cylindrical vacuum cavity (Region 2) is carved out of a metal block that fills solution volume (Region 1). The element size is 0.5 cm. The main difference is that the mesh contains two source regions at positions $x = \pm 7.0$ cm, $y = 0.0$ cm. A single source would drive electric field on only one side, resulting in a slight asymmetry of the field pattern.

Table 6 shows the full input script for the RF mode calculation. Note that we use the long form of the *NPeriod* command:

```
NPeriod  13  3  10
```

The first integer parameter designates a total run time $t_{max} = 13\tau$, where τ is the RF period at 1.219 GHz, 0.8203 ns. The second parameter specifies that the harmonic drive current should rise smoothly over the interval $0 \leq t \leq 3\tau$. The smooth start prevent the generation of high-frequency noise associated with discontinuities. The third parameter states that the drive current should drop to zero during the interval $7\tau \leq t \leq 10\tau$. If we did not terminate the drive current before the end of the run, the field amplitudes would rise throughout the run. in this case, the system would not be in a steady state at the time of conversion to phasor representation. The following *Source* commands set the proper phases of the sources at $x = \pm 7.0$ cm to drive the TM_{110} mode:

```
Jz(3,1) = 1.0
Jz(4,2) = 1.0
SMod(1) 0.0
SMod(2) 180.0
```

Figure 10 shows $H_y(t)$ at the origin over the length of the run. The signal illustrates that the fields achieve a steady-state at a single frequency. Figure 11 shows the variation of $|\mathbf{H}|$ over a plane normal to z along with vectors to indicate the direction of the magnetic field. -

Table 6: Contents of the **Aether** script `TM110.AIN`

```
* ---- CONTROL ----
Mode = RF
Mesh = TM110
DUnit =  100.0
Freq   1.2190E+09
NPeriod  13  3  10
* ---- SOURCES ----
Jz(3,1) = 1.0
Jz(4,2) = 1.0
SMod(1) 0.0
SMod(2) 180.0
* ---- REGION PROPERTIES ----
Metal(1)
Vacuum(2)
Vacuum(3)
Vacuum(4)
* ---- DIAGNOSTICS ----
History =   0.000  0.000  0.000

EndFile
```

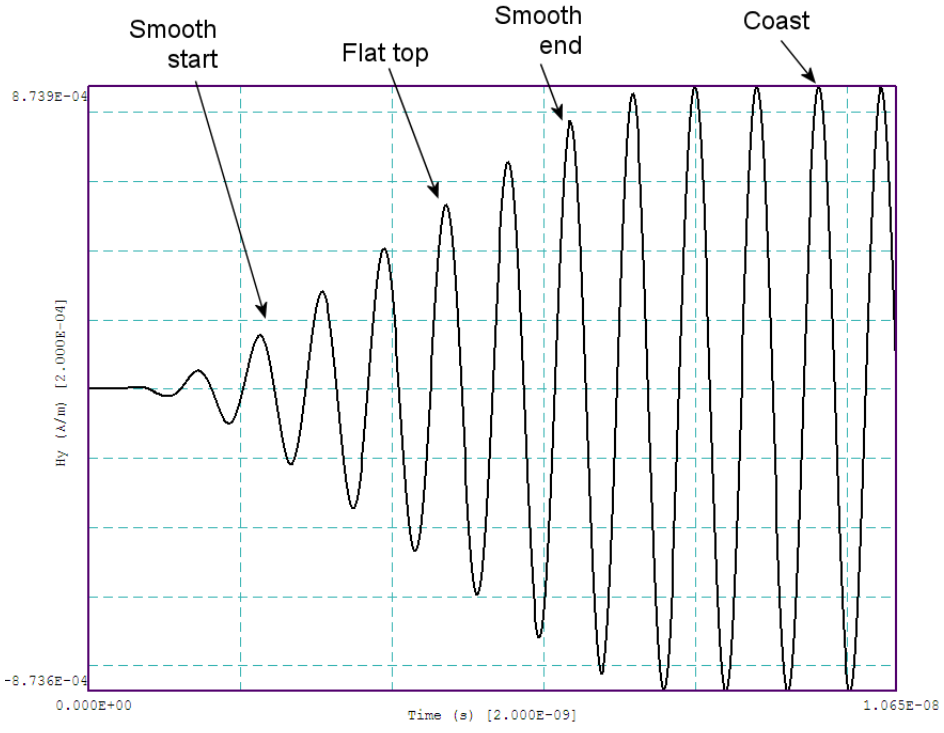

Figure 10: TM_{110} mode. Measurement of $H_y(t)$ at the origin.

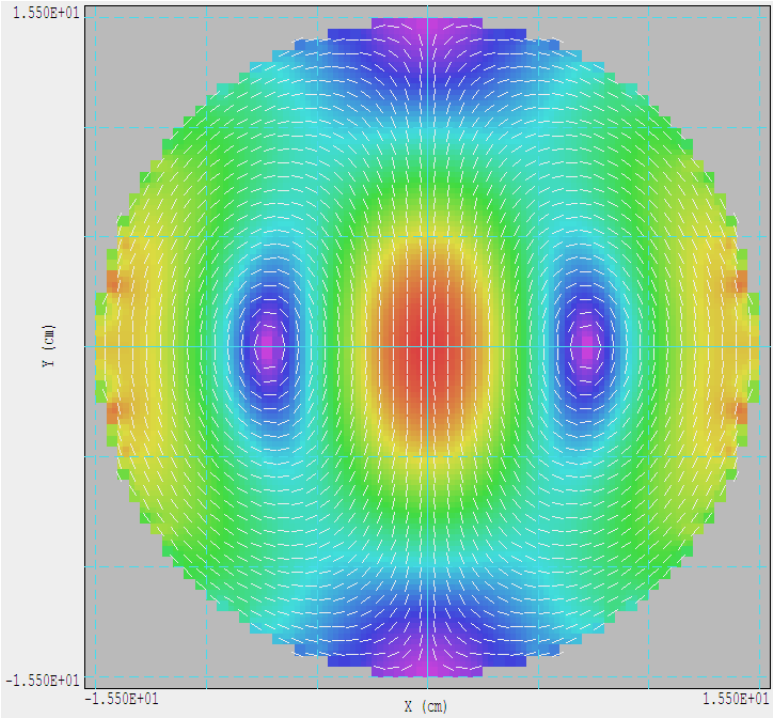

Figure 11: TM_{110} mode. Color-coded plot of $|\mathbf{H}|$ in the x-y plane with vectors to show the magnetic-field direction.

To conclude, it is important to emphasize that this example shows how to excite a mode in a high-Q resonator. Here, the exact location of the sources is not critical. The strategy is to activate drive currents for a limited time and then to allow the field to settle into an equilibrium. Strongly-damped structures (such as the driven coaxial transmission line of Tutorial 2) require a different approach. In this case, the spatial variations of source current must approximate those of the physical system. The time variation is a steady-state excitation at a single frequency following a smooth start.

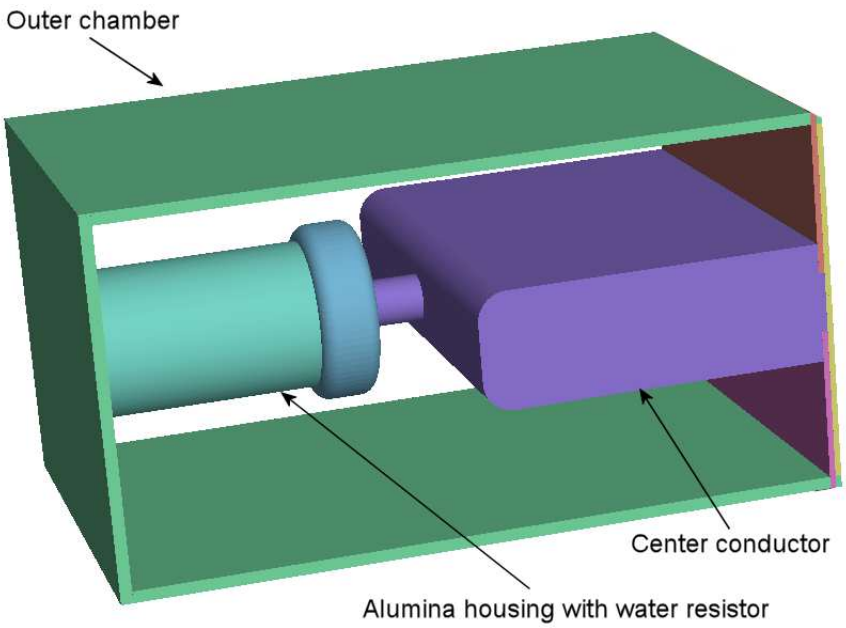

Figure 12: Three-dimensional view of the assembly. Pulse propagates along z (right to left). The y axis is vertical and x points out of the page. The system is periodic along the x direction.

5 Resistive load for a pulsed-power system

In this example, we shall use **Aether** to characterize a pulsed power system, making full use of the code's three-dimensional capabilities. The goal is to design a dummy load to test a low-impedance generator that drives a long parallel-plate transmission line. The design of the load resistor is a rather poor one to illustrate how the code can highlight problems. The example highlights two **Aether** techniques: 1) modeling a portion of a long periodic system using symmetry boundaries and 2) generation of pulse with desired properties in a transmission line.

Figure 12 shows the geometry described by the file `pulsedpower.min`. The transmission line has a long length along x (out of the page). The load consists of a series of identical resistors. The length along x of one cell $b = 8.0$". The spacing between the inner and outer conductors of the transmission line is $a = 2.0$". The resistive solution inside the alumina housing has radius $r = 0.875$" and length $L = 4.0$". Most of the assembly volume is filled with purified water. A voltage pulse of magnitude $V_0 = 1.2$ MV and risetime $t_r = 3.0$ ns is incident from the right-hand side.

Although only a short length ($L = 6.0$") of the transmission line is included in the model, we would like the line to behave as though it extended an infinite distance beyond the right-hand border. The technique is to include a termination layer on the boundary and to excite the pulse with an internal current source. Reflected pulses pass through the source and are absorbed by the layer. Figure 13, a two-dimensional projection in the plane $x = 0.0$", illustrates the computational mesh and the regions of the calculation. An element size of 0.10" gives a good representation of the curved surfaces. The mesh contains about 600,000 elements. The

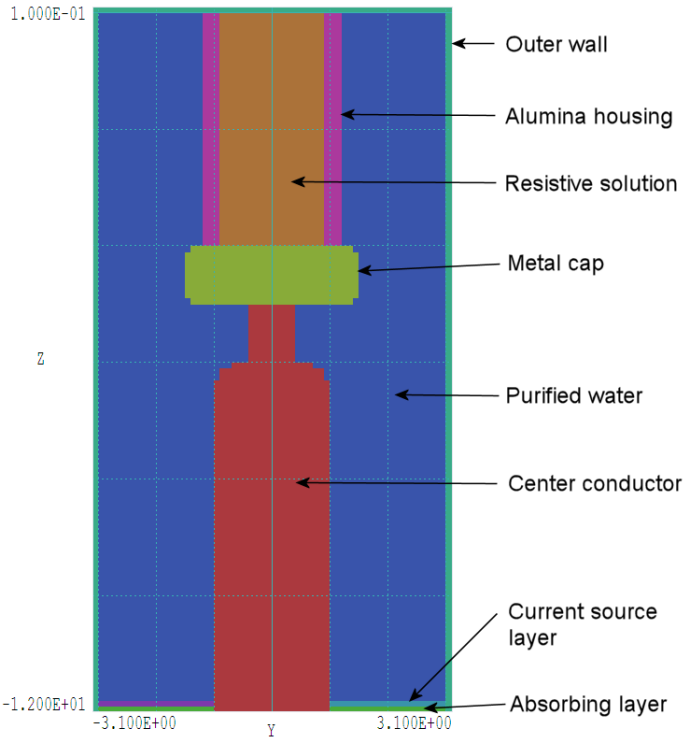

Figure 13:

outer wall, center conductor, metal cap and connecting rod are represented as metals in the **Aether** calculation. The purified water and resistive solution have $\epsilon_r = 81.0$, while alumina has $\epsilon_r = 7.8$. We need to determine two quantities: 1) the current density of the source layer to produce a 1.2 MV pulse and 2) the conductivity of the resistive solution for a matched termination.

The impedance of purified water is $\eta = 377.3/\sqrt{81} = 41.922\,\Omega$. The characteristic impedance of a section of the dual-sided parallel-plate transmission line of length b is

$$Z_0 = \eta \left(\frac{a}{2b}\right) = 5.2403\ \Omega. \tag{10}$$

For a 1.2 MV pulse, the source should supply a total current $2V_0/Z_0$, where half the current travels down the line and half is lost to the absorbing layer. Inserting values, the peak total current is 458.0 kA. Therefore, the current in the top and bottom source regions should have peak magnitude $I = 229.0$ kA. The source has dimensions 0.1" by 8.0", so the cross-section area is 5.161×10^{-4} m^2. The peak current density magnitude is therefore $j_y = 4.437 \times 10^8$ A/m^2. The cylindrical load has resistance

$$R = \frac{L}{\sigma \pi r^2}. \tag{11}$$

Taking R = 5.2403 Ω and inserting the dimensions, we find that the matched conductivity is $\sigma = 12.49$ S/m.

Table 7: Input script `pulsedpower.ain`.

```
* ---- CONTROL ----
Mode = Pulse
Mesh = PulsedPower
DUnit =  3.93700E+01
TMax =  3.010000E-08
SymBound XDn
SymBound XUp
* --- CURRENT SOURCES ---
SMod(1) = STEP 0.0 3.0E-9
* ---- REGION PROPERTIES ----
*     1      WATER
Epsi(1) =  8.10000E+01
*     2      ALUMINA
Epsi(2) =  7.80000E+00
*     3      RESISTOR
Epsi(3) =  8.10000E+01
Sigma(3) =  12.49
*     4      ABSORB
AbsLayer(4) 0.10 81.0 1.0
*     5      SOURCEUP
Epsi(5) =  8.10000E+01
Jy(5,1) = -4.437E8
*     6      SOURCEDN
Epsi(6) =  8.10000E+01
Jy(6,1) =  4.437E8
*     7      INNERCONDUCT
Metal(7) 81.0 1.0
*     8      RESISTPLATE
Metal(8) 81.0 1.0
*     9      OUTERBOUND
Metal(9) 81.0 1.0
* ---- DIAGNOSTICS ----
DTime =  5.00000E-09
* Inside resistor
History =   0.00000E+00  0.00000E+00 -2.0000E+00
* Midpoint of line
History =   0.00000E+00  2.00000E+00 -9.00000E+00
EndFile
```

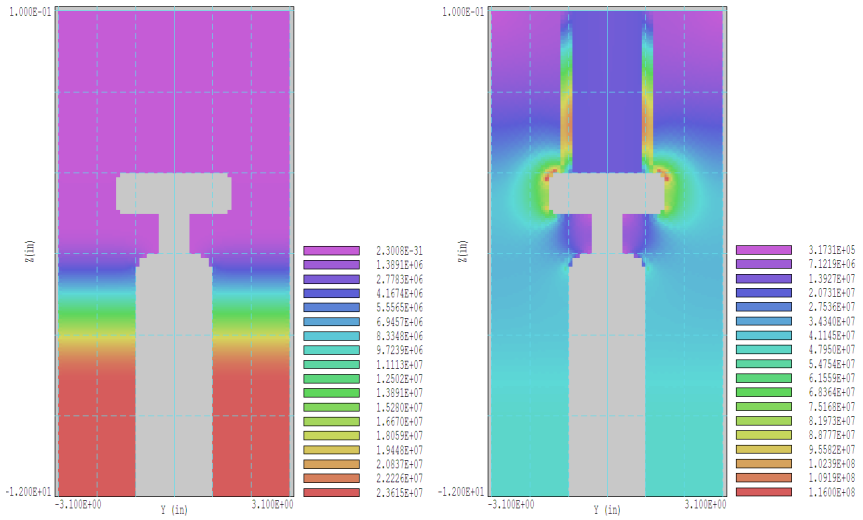

Figure 14: Distribution of $|\mathbf{E}|$, views in the plane $x = 0.0$". Left: $t = 5.0$ ns. Right: $t = 20.0$ ns.

Table 7 shows the complete input script. Some entries are of interest:

- The simulation time is 30.1 ns, long compared to the transit time of 4.57 ns along the 6.0" length of transmission line.
- The *SMod* command invokes the standard normalized *Step* function starting at $t_s = 0.0$ ns with a risetime of $t_r = 3.0$ ns.
- The upper and lower boundaries along x are set as symmetry planes. The assignment is valid because 1) pulse propagation is parallel to the planes and 2) the magnetic field is symmetric about the planes.
- The two source regions have the dielectric constant of water and peak current densities $j_y = \pm 4.437 \times 10^8$ A/m^2.
- Snapshots of the field distribution are recorded at 5.0 ns intervals, and probes are located at the midpoints of the transmission line and resistor.

The **Aether** run takes about 5 minutes. Figure 14 shows the electric field distribution in the plane $x = 0.0$" at $t = 5.0$ ns and $t = 20.0$ ns. The early-time plot shows the initial plane pulse moving down the line. The field magnitude agrees with the theoretical prediction, $|E_y| = V_0/a = 2.362 \times 10^7$ V/m. The view on the right shows the distribution at $t = 20.0$. The reflected pulse in the transmission line indicates that there is a poor impedance match. Another concern is the strong concentration of electric field on the resistor end cap and across the insulator housing. Finally, probe signals plotted in Fig. 15. There is a large reflected pulse in the line and the resistor current rises slowly. The resistor provides a poor match to the fast-rising pulse. The cause of the problem is the high inductance of the small-radius connecting rod and resistive solution.

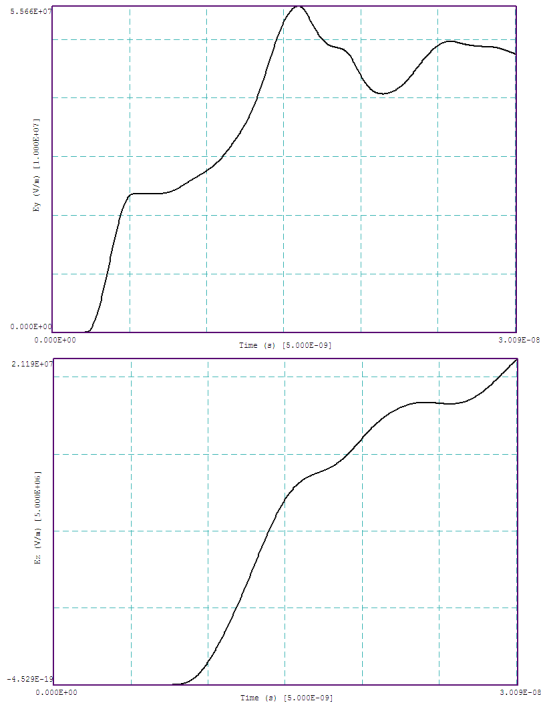

Figure 15: Probe signals. Top: midpoint of transmission line, $E_y(t)$. Bottom: midpoint of resistor, $E_z(t)$.

6 Radiation from a simple dipole

This example provides an opportunity to check the accuracy of **Aether** in a radiation calculation in the *RF* mode and also to try some useful features of the **Aerial** post-processor. We shall consider a simple dipole antenna that consists of a region of height h that carries a current of amplitude I_0 oscillating at frequency f. The file `SIMPLEDIPOLE.MIN` describes a dipole oriented along z with $h = 0.06$ m and cross-section area $A = 4.0 \times 10^{-4}$ m^2. A current density of amplitude $j_z = 1.0$ A/m^2 gives $I_0 = 4.0 \times 10^{-4}$ A. In the limit that the dipole height is small compared to the radiation wavelength λ, the predicted time-averaged radiated power is:

$$P = 40\pi^2 I_0^2 \left(\frac{h}{\lambda}\right)^2 . \tag{12}$$

For the choice $f = 0.6$ GHz, the wavelength is $\lambda = 0.4997$ m. Inserting values in Eq. 12, the predicted power is 9.107×10^{-7} W.

The solution volume is a cube with sides of length 102.0 cm. The element width is 1.0 cm. An outer layer (Region 1) of thickness 1.0 cm is set as an ideal absorber. The vacuum volume is divided into two parts: a cubic box with 100.0 cm sides (Region 2) and a sphere of radius 35.0 cm (Region 3). The reason for the division will be apparent in the discussion of **Aerial** plots. Finally, Region 4 is a vacuum box of width 2.0 cm in x and y and height 6.0 cm in z. The **Aether** calculation is controlled by the file `SIMPLEDIPOLE.AIN`. The run extends over 6 RF periods with a smooth start of 2 periods. The statements

```
SMod(1) = 0.0
Jz(4,1) = 1.0
```

define a current-density amplitude of 1.0 A/m^2 with phase 0.0^o in Region 4. Monitors to check the convergence of the time-domain solution are located at position $[25.5, 0.0, 0.0]$. The solution takes about 5 minutes.

One way to check the radiated power is to inspect the volume-integral table recorded in `SIMPLEDIODE.ALS`. The time-averaged power dissipated in the absorber (Region 1) is $P = 9.181 \times 10^{-7}$ W, within 0.8% of the theoretical value. We can also load the solution file `SIMPLEDIODE.AOU` into **Aerial**, open a data record and then pick the command *Analysis/Solution integrals*. **Aerial** lists surface integrals of the Poynting vector in addition to the same volume integrals performed by **Aether**. The results, shown in Table 8, are listings of the flow of electromagnetic energy out of regions through boundaries shared with other regions. It is informative to discuss the features and limits of the analysis. The main concern is that the field quantities are evaluated at the centers of boundary elements of the region. Therefore, results are not accurate for regions with a single layer of elements. In this case, there are large changes of field values over single elements. For example, the entries in Table 8 for Region 1 show power $P/2$ arriving from Region 2 and $P/2$ leaving through the outer boundary of the solution volume (designated as Region 0). In reality, the power P arrives from Region 2 and is fully dissipated in the absorber. Poynting integrals of the power from Region 2 to the absorber and from Region 3 to Region 2 are in good agreement with the volume-integral results. Finally, integrals over

Table 8: **Aerial** surface integral results

```
Time-averaged Poynting vector flux
  Power from region:   1
     RegNo >>   0   Area:   6.24240E+00 (m2)    Power:   4.59177E-07 (W)
     RegNo >>   2   Area:   6.00000E+00 (m2)    Power:  -4.56835E-07 (W)
  Power from region:   2
     RegNo >>   1   Area:   6.00000E+00 (m2)    Power:   9.23561E-07 (W)
     RegNo >>   3   Area:   2.31121E+00 (m2)    Power:  -9.09663E-07 (W)
  Power from region:   3
     RegNo >>   2   Area:   2.31121E+00 (m2)    Power:   9.23431E-07 (W)
     RegNo >>   4   Area:   5.60003E-03 (m2)    Power:  -6.72397E-07 (W)
  Power from region:   4
     RegNo >>   3   Area:   5.60003E-03 (m2)    Power:   4.70630E-07 (W)
```

the surface of Region 4 are inaccurate because of the strong field variations over the surface of the small object.

Aerial can generate a variety of interesting plots. We shall consider two examples created in the *Surface plot* menu. Figure 16 was generated with the following operations:

1. In the *Surface plot* menu, pick the *Display regions* command. In the dialog, check *Display* for Regions 2 and 4 and check *Field* for Region 2.

2. Pick the *Set cut planes* command. In the dialog, set $y_{min} = 0.0$ cm.

3. Pick the *Surface plot style* command. In the dialog, uncheck the box *Include surface plot.*

The resulting plot of $|\mathbf{H}|$ in Fig. 16 shows the standard dipole pattern with radiated fields concentrated at the equator.

Figure 17 shows how three-dimensional field lines may be added to surface plots. To prepare, deactivate the display of Region 2 with the *Display regions* command and check the box *Include surface plot* in the *Surface plot style* dialog. Create the plot with the following operations:

1. Click *Reference phase/amplitude* to toggle the display mode. Use *Set reference phase* and enter a value $\phi = 90^{\circ}$. The plot surface now shows a snapshot of the fields at the specified phase. The choice of 90°ensures that the near-fields around the dipole are close to zero and do not obscure the radiating fields.

2. The surface shows the variation of $|\mathbf{H}$ over a plane normal to z. In the *Surface plot style* dialog, change the position of the plot surface to $z = -5.0$ cm so it is below the dipole region.

3. We can add field lines to surface plots in the *Reference* display mode. Pick the command *Field line plot file* in the *Analysis* menu. In the dialog, choose the file `DIPOLELINES.DAT`. It contains a list of starting positions for field line traces.

The surface in Fig. 17 is color-coded according to the default plot quantity $|\mathbf{H}|$. By default, the lines follow $\mathbf{E}$ vectors. The starting positions are a sequence along the x axis at $y = 0.0$ cm,

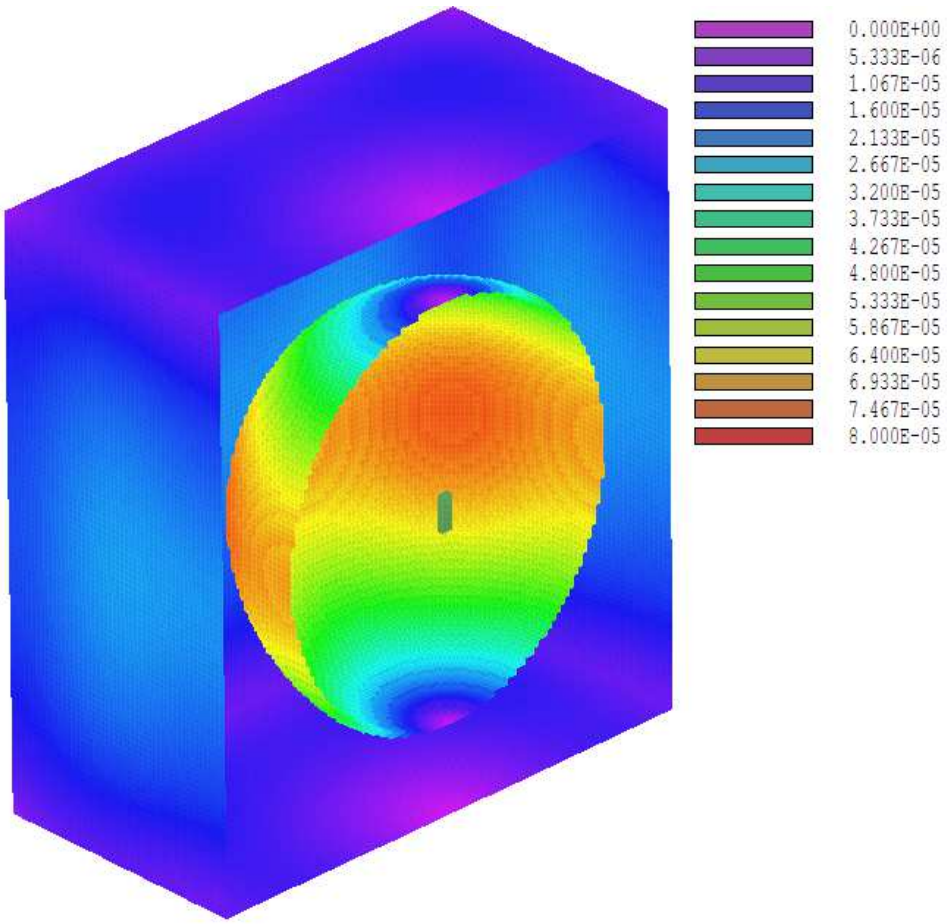

Figure 16: Amplitude plot of $|\mathbf{H}|$ on the surface of a sphere of radius 35.0 cm and on the boundary of the absorbing layer. The green object is the dipole region.

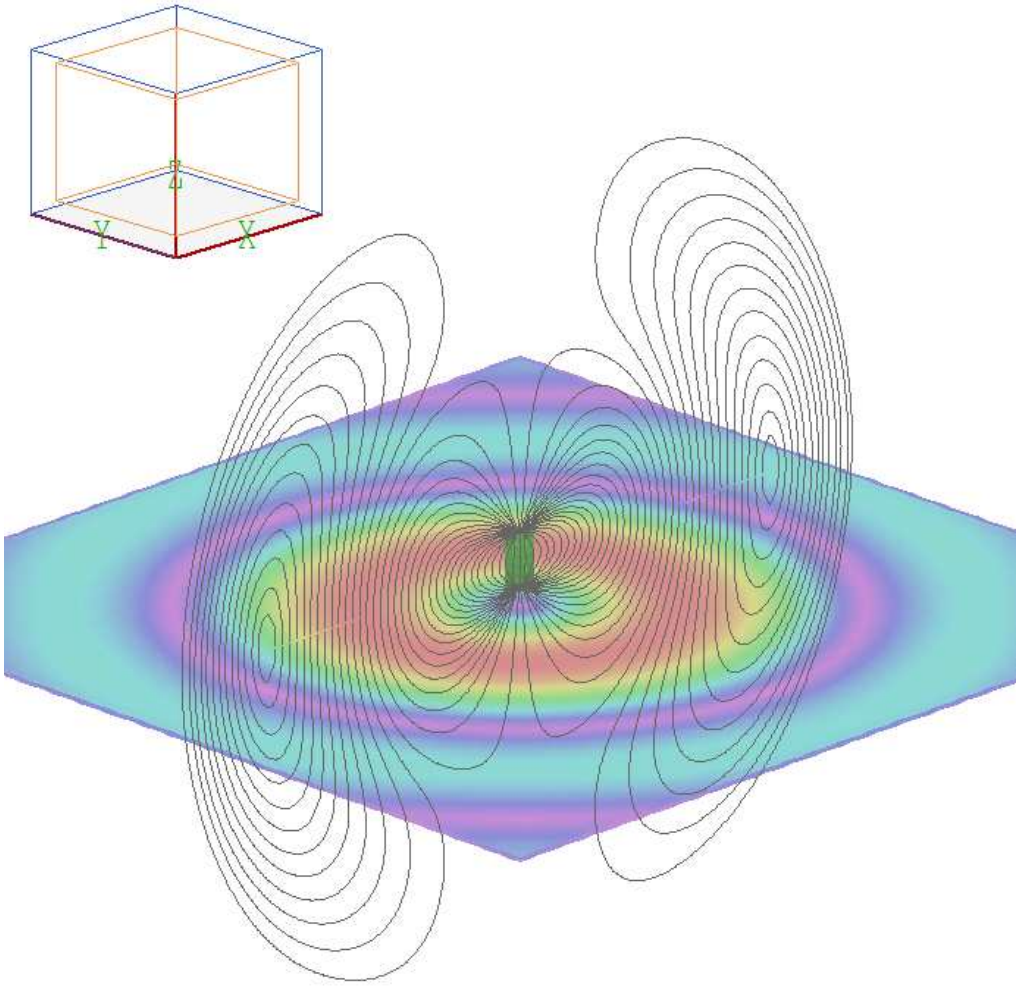

Figure 17: Color-coded plot of $|\mathbf{H}|$ over a surface at $z = -5.0$ cm at phase $\phi = 90^{\circ}$. Lines of electric field in the plane $y = 0.0$ cm.

$z = 0.0$ cm. Note that **Aerial** traces lines until they leave the solution volume or reconnect with themselves. The starting positions in `DIPOLELINES.DAT` are in the range $|x| \leq 35.0$ cm. A larger limit would have resulted in doubling of lines in some regions.

7 Switching transmission lines and capacitors

Many pulsed-power systems include static or pulse-charged transmission lines that are discharged by a fast switch. Electromagnetic interference applications may involve a capacitor discharge. In both cases, the initial state has large electric fields and small or zero magnetic fields. The question is how to create a static initial state with a dynamic electromagnetic code using currents as drive elements. This example illustrates the solution. The geometry is simple to allow comparisons with theory. Nonetheless, the example illustrates all aspects of switch modeling and can provide an important template for your work.

Figure 18 shows a cross-section of the system, two parallel-plate transmission lines separated by a switch region. The charge line is at the bottom and the output line at the top. The system is uniform in x and has length 10.0 cm out of the page. The key to the calculation is the assignment of a time-dependent conductivity to the switch region. The conductivity is zero while the lower line is charged and then rises rapidly to a high value to drive a pulse in the output line. The calculation includes several regions:

- Outer conductors at y_{min} and y_{max} which have the *Metal* property.
- The inner conductors of the charge and output lines (*Metal*).
- The line media, which have the properties of vacuum ($\epsilon_r = 1.0$, $\mu_r = 1.0$.)
- Matched resistive layers at z_{min} and z_{max} (*AbsLayer*).
- Two drive current layers near z_{min} with oppositely-directed currents ($\pm j_y$).
- The switch region with time-dependent σ.

The distance between the center and outer conductors is $a = 2.0$ cm. The characteristic impedance of the line section of width $b = 10.0$ cm is 37.3 Ω (Eq. 10). The electromagnetic transit time over the 25 cm length of the charge line is 0.833 ns, short compared to the charge time of 3.0 ns. The risetime of the current density is 0.5 ns. The source and absorption layers have thickness $\Delta z = 0.5$ cm. A peak current density $j_y = 1.0$ A/m^2 in the left and right source regions produces a total current

$$I = 2 j_y b \Delta z = 0.001 \text{ A}, \tag{13}$$

of which half is lost to the adjacent absorption layer. The current produces a traveling pulse with field amplitude $E_{y0} = 0.933$ V/m.

The switch region has length 5.0 cm, width 10.0 cm and height 2.0 cm. With these dimensions, a conductivity $\sigma = 25.0$ S/m in the conducting phase gives a switch impedance of 1.0 Ω. The following lines in the **Aether** control script `EINIT.AIN` are used to define the switch properties:

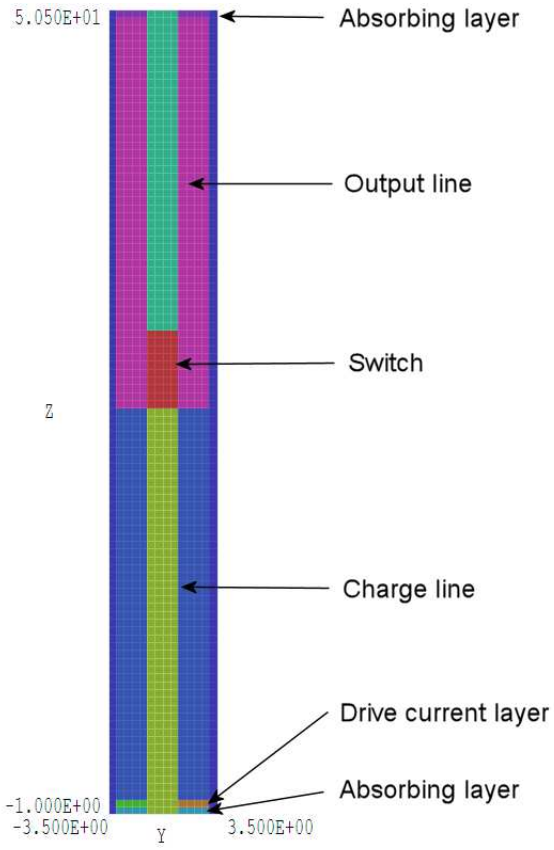

Figure 18: Geometry of the `EINIT` example, view normal to the x axis. The dimensions are in cm. The system is uniform along x with length 10.0 cm and symmetry boundaries at x_{min} and x_{max}

.

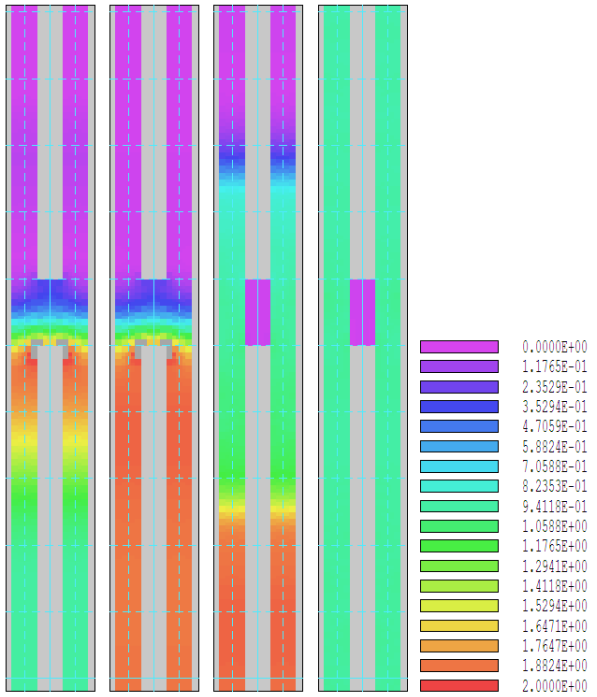

Figure 19: Plot of $|\mathbf{E}|$ in the plane normal to x at times $t = 1.5$, 3.0, 3.5 and 5.0 ns.

```
Epsi(7) = 1.0
Mu(7) = 1.0
Sigma(7) = 25.00
SigMod(7) = EINIT.DAT
```

The *Sigma* statement sets the peak magnitude of the conductivity as $\sigma = 25.0$ S/m. The *SigMod* statement signals that the conductivity has a time dependence defined by the table `EINIT.DAT`. The file contains a normalized function that equals 0.0 for $t < 3.0$ ns and then rises smoothly to 1.0 over a 1.0 ns interval.

Figure 19 shows the spatial variation of electric-field at selected times. In the first plot, a wave of voltage amplitude $V_0/2$ has moved into the charge line and partially reflected to create a region of V_0. The second plot (just before switching) shows the line fully charged to V_0. The distribution of electric field is almost identical to an electrostatic solution with the center conductor at potential V_0. In the third plot, the switch region has high conductivity. A pulse with voltage $V_0/2$ moves into the output line and a $-V_0/2$ pulse moves backward in the charge line. The last segment shows the steady state where a $V_0/2$ pulse fills the solution volume.

Figure 20 shows the variation $E_y(t)$ measured with a probe at the midpoint of the charge line. The signal changes to E_{y0} at the onset of the primary pulse and then to $2E_{y0}$ with the addition of the pulse reflected from the open-circuit switch. The field remains at an approximately static level until activation of the switch, after which is returns to E_{y0}.

The small transients at full charge in Fig. 20 illustrate an interesting aspect of numerical solutions: it is easy to represent a real-world system, but rather difficult to create an ideal solution. In a model of a pulse-charged Blumlein line, **Aether** gives a complete representation with actual transients included. As a final note, you must take care to include reasonable risetimes in temporal functions. If the drive current function in the example were a discontin-

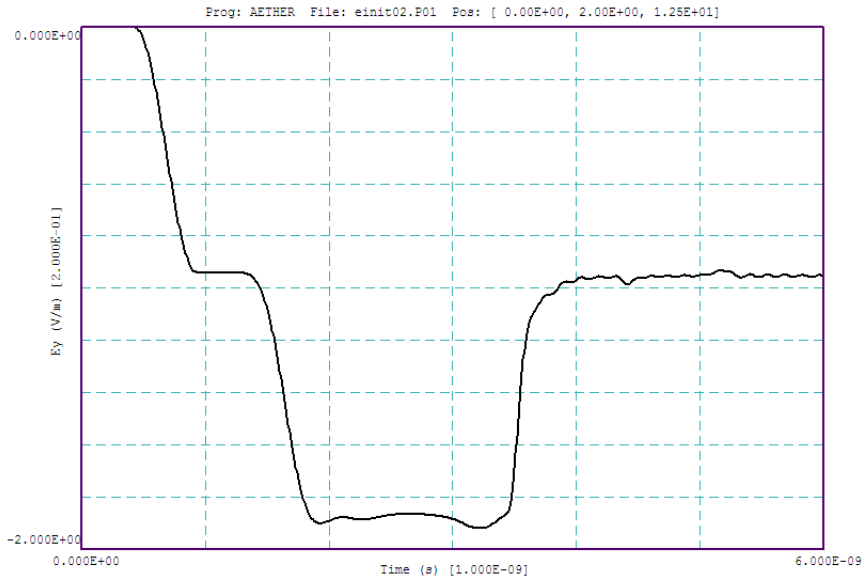

Figure 20: Plot of $E_y(t)$, signal from a probe at the midpoint of the charge line.

uous step function, there would be large transients in the charge phase. Even more critical, a discontinuous function for the switch conductivity would yield a non-physical solution.

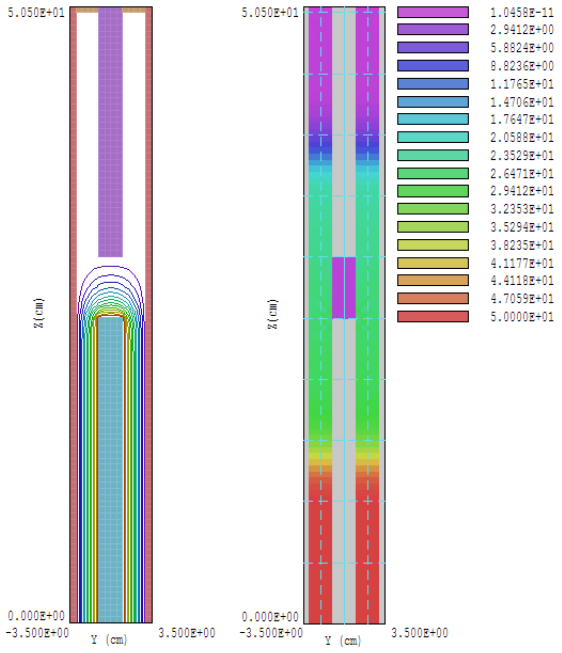

Figure 21:

8 Initial electric-field distributions from HiPhi

The initial static electric field distribution in devices like charged transmission lines, Blumlein lines and capacitors may have complex three-dimensional variations. Setting the initial electric field with the charging method described in Chap. 7 can be time-consuming. If you have the **HiPhi** code, you can set electric fields at $t = 0.0$ s directly from an electrostatic solution. The two examples of this section demonstrate how to implement the technique:

- `EBIAS`. This example is a simple benchmark for comparison to theory. The geometry show in Fig. 21 is the same as that of the `EINIT` example in Chap. 7. The calculation employs the input files `EBIAS.MIN` (mesh geometry), `EBIAS.HIN` (**HiPhi** control), `EBIAS.DAT` (time variation of switch conductivity) and `EBIAS.AIN` (**Aether** control).

- `DTESTER`. A full three-dimensional simulation of a device to test dielectric breakdown under severe voltage reversal conditions. This calculation would be impossible without **Aether**. The input files are `DTESTER.MIN`, `DTESTER.HIN`, `SMOOTHSTEP.MOD` and `DTESTER.AIN`.

Figure 21 shows the geometry of the `EBIAS` example. The figure shows the view in the plane $x = 0.0$ cm for a parallel-plate vacuum transmission line with infinite length along x. The center conductor of the charge line (lower portion) has a static charge of 1.0 V. The line has length 25.0 cm and gap width 2.0 cm. The initial electric field is $E_{y0} = 50.0$ V/m. The upper portion of the solution volume is an output line with a matched termination layer. The center

conductors of the lines are connected by a switch region of length 5.0 cm that undergoes a rapid rise in conductivity in the electromagnetic calculation.

The first task after generating the mesh is to create the electrostatic solution. In the **HiPhi** calculation, the outer wall, the output line center-conductor and the downstream absorber are set to $\phi = 0.0$ V. The center conductor of the charge line is set to $\phi = 1.0$ V. The line volume and switch have $\epsilon_r = 1.0$. The lower end of the charge line has an unspecified boundary which corresponds to an open-circuit boundary condition in both **HiPhi** and **Aether**. The left-hand side of the figure shows calculated equipotential lines which extend across the open-circuit switch in the initial state. The following command in the **Aether** script loads the electrostatic solution `EBIAS.HOU`:

```
Einit EBias
```

Note that there are no instances of the *SMod*, *Jx*, *Jy* and *Jz* commands in the script because the dynamic solution does not require current sources.

There are two important considerations for importing **HiPhi** solutions into **Aether**:

- The two programs must use the same mesh. You should plan the division into regions so that the mesh serves both the electrostatic and electromagnetic solutions. The mesh must be non-conformal. The mesh script should include the command *Smooth 0* and should not include *Surface* commands.
- For a valid physical solution, the initial state of the electromagnetic solution must be consistent with the electrostatic solution. In this example, the switch region has the same dielectric constant and has $\sigma = 0.0$ S/m at $t = 0.0$.

The function in the file `EBIAS.DAT` and the command *Sigma(4) = 25.00* define a smooth change of conductivity from 0.0 to 25.0 S/m in 1.0 ns. As in the example of Chap. 7, non-physical results may occur if the conductivity changes discontinuously or abruptly compared to the time step of the solution. The right-hand side of Fig. 21 shows the spatial distribution of $|\mathbf{E}|$ at $t = 0.5$ ns. As expected, waves with electric field magnitude $E_{y0}/2$ move away from the switch. The pulse in the output line has magnitude slightly below 0.5 V and duration 1.76 ns (full-width at half maximum). For comparison, the double transit time in a vacuum line of length 25 cm is 1.67 ns, so the non-zero switching time gives some pulse lengthening.

Figure 22 shows the geometry of the `DTESTER` example. The goal is to determine the effect of strong voltage reversal on the lifetime of a dielectric sheet. The plate and inductor are charged to a high static voltage. A switch shorts the electrodes, generating a oscillating voltage across the sheet. The assembly is immersed in transformer oil inside a grounded tank (a cube with sides of length 15.0 cm). Three-dimensional numerical methods are essential for this calculation for three reasons:

- The initial electric field distribution is quite complex.
- The effect of the tank walls and electrodes makes it difficult to estimate lumped element parameters.
- Transit-time effects play a large role in determining the electric field in the test insulator.

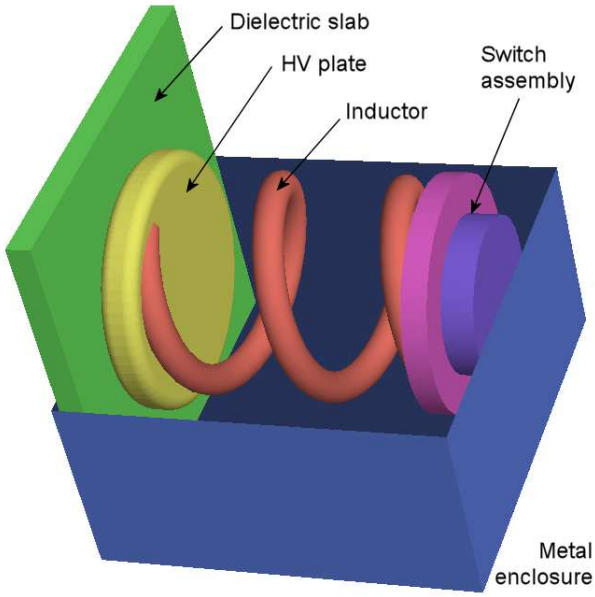

Figure 22: Geometry of the DTESTER example.

The left-hand side of Fig. 23 shows the spatial distribution of $|\mathbf{E}|$ for a normalized electrostatic solution with 1.0 V applied potential. The electric field magnitude is 50 V/m across the dielectric slab of thickness 1.0 cm and the switch. There is field enhancement on the edges of the high-voltage, so it would be worthwhile to refine the shape. The dielectric has $\epsilon_r = 5.8$ and the oil has $\epsilon_r = 2.7$. The dielectric constant of the switch material has little effect on either solution, for we set it to the value for oil to maximum the Courant time step.

In the electromagnetic solution, the switch again has an initial conductivity of zero and rises to 25.0 S/m in 5 ns. The command to set the time variation is:

```
SigMod(4) = SMOOTHSTEP.MOD 5.0E-9 1.00
```

where the file SMOOTHSTEP.MOD contains a normalized function that rise smoothly to 1.0 at t = 5.0 s. The right-hand side of Fig. 23 shows the distribution of electric-field magnitude at t = 50.0 ns. The electric field energy is concentrated in the dielectric gap. The time-variation of electric field inside the dielectric is plotted in Fig. 24. The waveform is approximately sinusoidal function, as expected for an LC circuit. In contrast to the lumped-element solution, the electric field is larger on the negative cycle. This result reflects transit-time effects with pulse interference. Plots of $|\mathbf{H}|$ show that the magnetic field energy distribution along the helical inductor varies with time. We could determine capacitance and inductance values of the assembly with an *RF mode* calculation. For a rough estimate, note that the dielectric gap has spacing 0.01 m and approximate area 7.85×10^{-4} m^2. The dimensions correspond to a capacitance of about 40.0 pF. The oscillation period is 20 ns, implying an inductance of 0.25 μH.

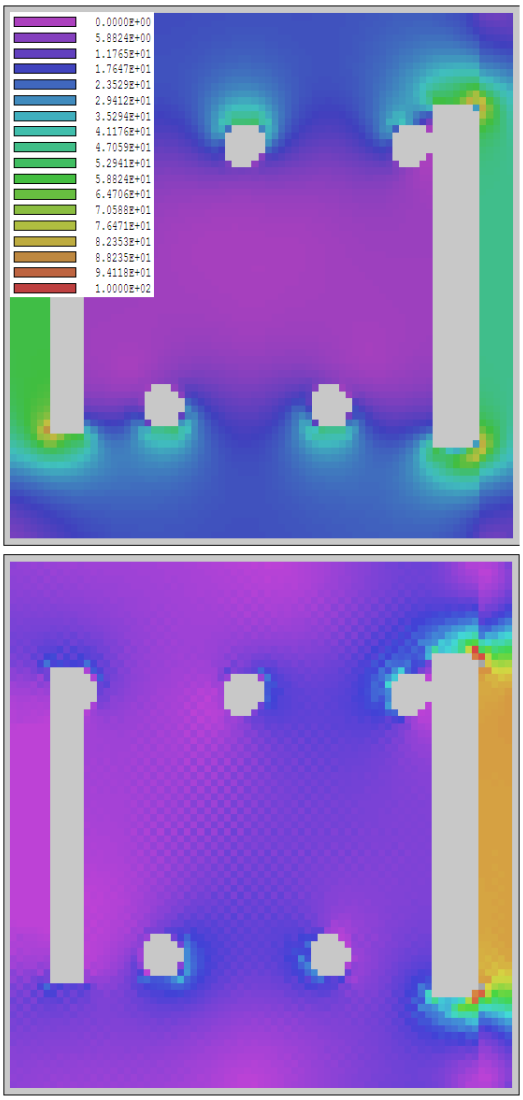

Figure 23: Spatial distribution of $|\mathbf{E}|$ in the plane $x = 0.0$ cm for the `DTESTER` example. Top: initial static field. Bottom: dynamic field at $t = 50.0$ ns

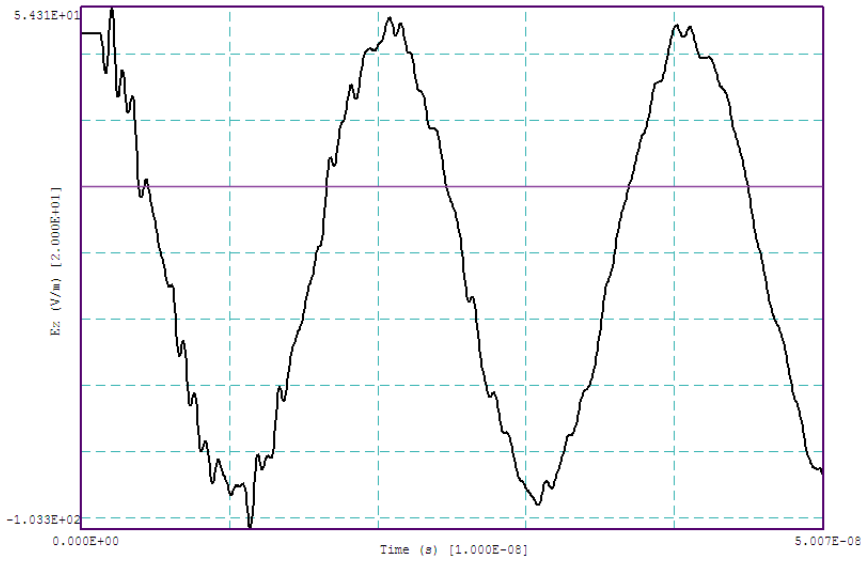

Figure 24: Plot of $E_z(t)$ at the center of the dielectric slab, `DTESTER` example.

9 TE10 mode in a rectangular waveguide

There are many applications that involve driving a microwave structure with a waveguide. This tutorial explains how to generate the TE_{10} mode in a rectangular waveguide. The method is applied in a three-dimensional application example, the design of a waveguide resonator for plasma heating.

In order to generate a single mode, we need some knowledge of the field pattern. Suppose that the waveguide extends along the z direction and has transverse dimensions $-a/2 \le x \le +a/2$ and $-b/2 \le y \le +b/2$. The TE_{10} mode has field components E_y, H_x and H_z that are uniform in y. The transverse components have spatial variation[1]:

$$E_y = E_0 \cos\left(\frac{\pi x}{a}\right), \tag{14}$$

$$H_x = -\left(\frac{E_0}{Z_E}\right) \cos\left(\frac{\pi x}{a}\right). \tag{15}$$

The mode impedance is given by

$$Z_E = \frac{\eta}{\sqrt{1-(\lambda/2a)^2}}, \tag{16}$$

where λ is the vacuum wavelength and η is the impedance of free space (376.7 Ω). The group velocity of the wave is

$$v_g = \frac{1}{\sqrt{\epsilon\mu}} \sqrt{1-(\lambda/2a)^2}. \tag{17}$$

For the initial calculation we shall use a vacuum waveguide with stock dimensions $a = 74.0$ mm and $b = 34.0$ mm. At frequency $f = 2.45$ GHz, the wave parameters are $\lambda = 122.4$ mm, $Z_E = 670.1$ Ω and $v_g = 0.5762c$. The mesh file `TE10.MIN` sets an element size of 1.0 mm and defines the following regions:

Region 1. Metal waveguide wall.

Region 2. Vacuum, interior of the waveguide.

Region 3. Top and bottom nozzles approximately one quarter wavelength from the end wall. This region acts as vacuum for the setup solution and as metal for the application solution.

Region 4. An absorbing layer with a spatial distribution of current density to drive the mode.

[1] Materials in this tutorial are taken from S. Ramo, J. Whinnery and T. Van Duzer, **Field and Waves in Communication Electronics** (Wiley, New York, 1965), Sect. 8.03

Region 5. The end wall. This region acts as an absorber for the setup solution and as metal for the application solution.

The solution volume covers the axial range -1.0 mm $\leq z \leq$ 151.0 mm.

The goal of the first solution (`TE10_01.AIN`) is to generate an ideal traveling wave. Equation 15 implies that the current density in the source region should have the spatial variation:

$$j_y = j_0 \cos(\pi x/a). \tag{18}$$

The distribution is implemented with the script command

```
Jy(4,1) > 1.0*cos(0.04245*\$x)
```

To begin, we simply set the properties of the source and downstream absorber regions with the commands:

```
AbsLayer(4) = 1.0
AbsLayer(5) = 1.0
```

In this case, **Aether** automatically assigns the conductivity $\sigma = 2.655$ S/m to the regions. The top section of Fig. 25 shows the spatial variation amplitude of the complex electric field. For an ideal traveling wave, there should be no variation in z. In contrast, the solution exhibits a high standing-wave ratio. We can understand this effect by noting that the assigned matched conductivity applies for waves at normal incidence ($\theta = 90^o$). As described in the **Aether Reference Manual**, the effective thickness of the layer increases when $\theta < 90.0$/dg. In this case, the conductivity should be multiplied by $\sin\theta$. The modes of a waveguide can be viewed as a superposition of waves that propagate at an angle with respect to the z axis given by

$$\sin\theta = v_g \sqrt{\epsilon\mu}. \tag{19}$$

For the parameters of the waveguide and mode, Eq. 19 implies the absorbing layers should have the conductivity $\sigma = 1.492$ S/m. The following commands explicitly set the properties of the layer regions:

```
Sigma(3) =   0.00000E+00
Epsi(4) =   1.00000E+00
Mu(4) =   1.00000E+00
Sigma(4) =   1.49200E+00
Epsi(5) =   1.00000E+00
Mu(5) =   1.00000E+00
Sigma(5) =   1.49200E+00
```

Conductivity matching is a subtle but critical point. The general rule is that you should always multiply the conductivity of absorbing layers in waveguide solutions by the ratio of the group velocity to the speed of light. The bottom of Fig. 25 shows the modified solution, almost a perfect traveling wave. Figure 26 shows a view of the fields at a reference phase $\phi = 0.0^o$.

To complete the discussion of the setup solution, consider the absolute amplitudes of the field quantities. The peak electric field amplitude in Fig. 25 is $E_0 = 0.43$ V/m. For a drive current density of 1.0 A/m^2, the maximum value of magnetic field is $H_{x0} \leq 0.001$ A/m. Using

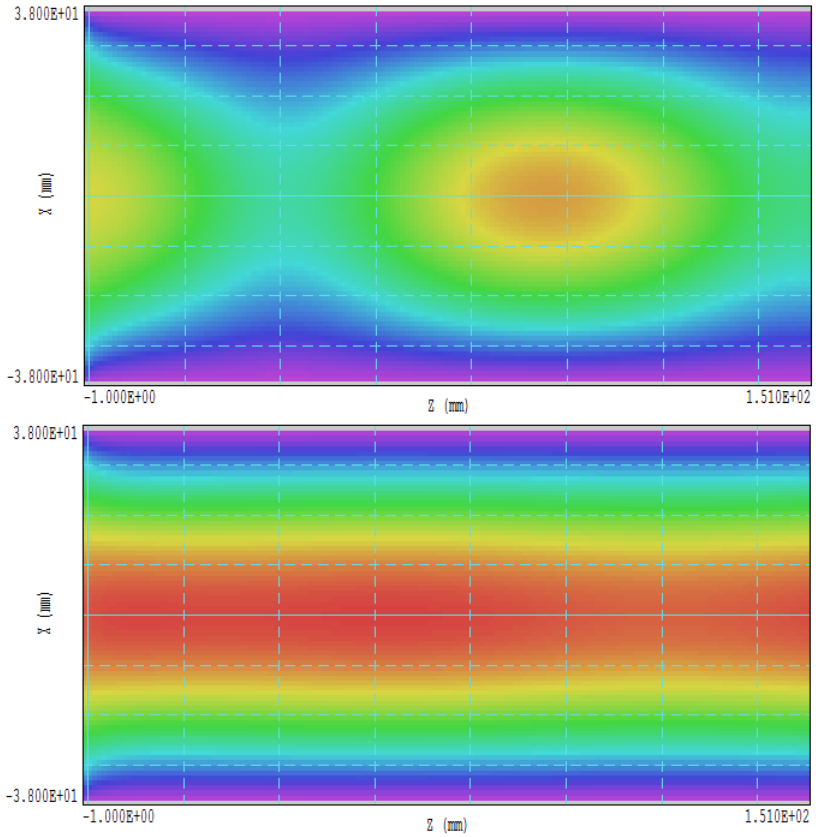

Figure 25: Traveling-wave solution, plot of $|\mathbf{E}|$ in the plane $y = 0.0$. Top: absorbing layer conductivity $\sigma = 2.655$ S/m. Bottom: absorbing layer conductivity $\sigma = 1.492$ S/m.

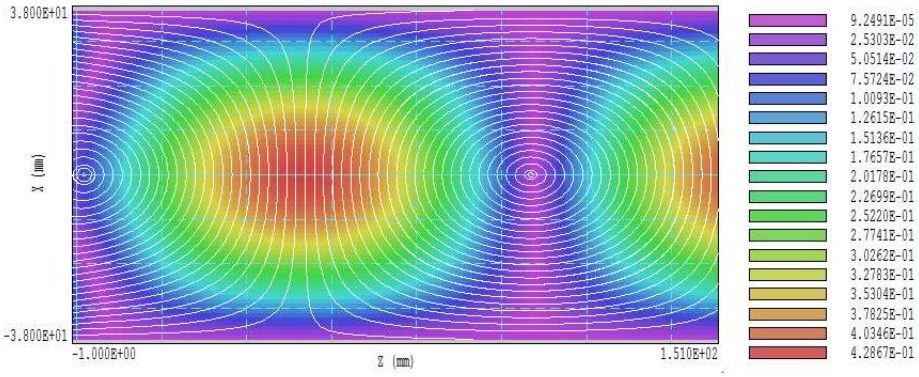

Figure 26: Field variations of the traveling-wave solution in the plane $y = 0.0$ at reference phase of 0.0°. Color coding by $|\mathbf{E}|$ with plotted lines of $|\mathbf{H}|$.

Eq. 15, the maximum electric field is $E_0 \leq 0.67$ V/m. The difference from the numerical solution arises from current-density cancellation in the source layer by ohmic conduction. For a matched conductor at normal incidence, the fractional backflow is usually 50%. The observed field reduction is about 64% because of the reduction in layer conductivity. The point is that it would be challenging to find the absolute field magnitude in a waveguide mode from first principles. It is simpler to set up a normalized solution and then adjust the current-density for the desired power. For this example, the total power calculated using the *Solution integrals* command in **Aerial** is 1.7×10^{-7} W. The peak voltage corresonding to $E_0 = 0.43$ V/m is $V_0 = 0.01462$ V, giving a predicted average power

$$P = \frac{V_0^2}{2Z_E} = 1.6 \times 10^{-3}. \quad \text{(W)} \tag{20}$$

As an application, we shall use a waveguide resonator to generate a strong RF electric field for gas ionization. The file `TE10_02.AIN` includes two changes from the setup solution:

The drive current density in renormalized to give an incident wave power flux of 1.0 kW.

The end wall and the region representing the nozzles is set to the metal condition.

The nozzles cylinders of radius 6.0 mm that extend 8.0 mm from the top and bottom surfaces of the waveguide. They are located 30 mm ($\lambda/4$) upstream from the end wall near the point of peak electric field. In addition to gas injection, they function to concentrate the electric field.

Figure 27 shows two views of the resulting electric field. The top illustration shows a strong standing wave pattern with enhanced electric field between the nozzles. The maximum field available for gas breakdown is 1.13 kV/cm.

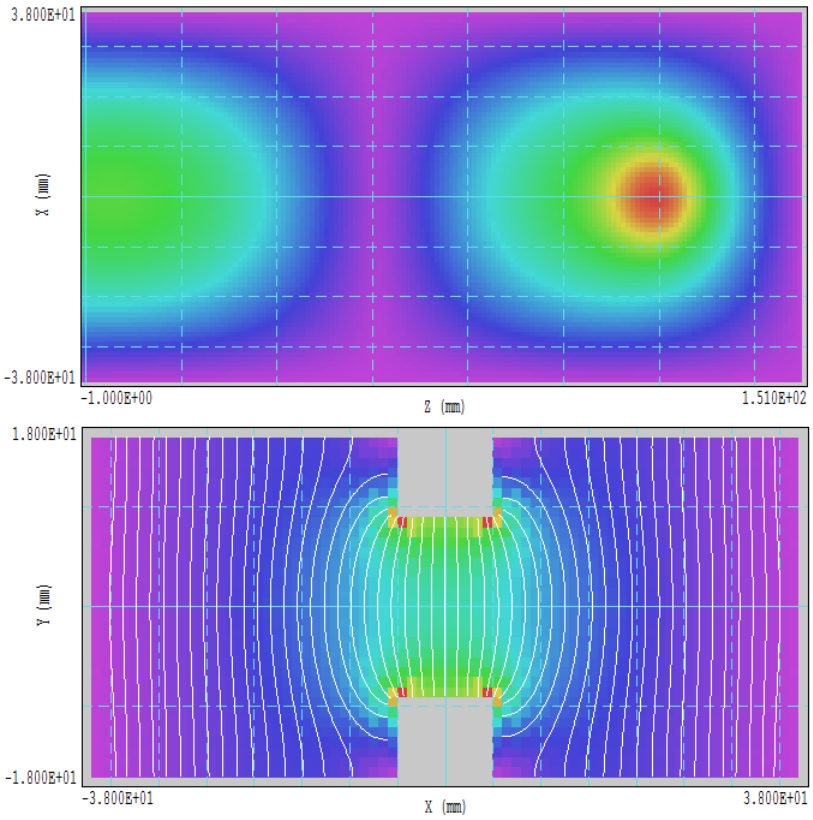

Figure 27: Waveguide cavity with gas nozzles, peak electric field 1.13 kV/cm. 1 kW incident power flux. Top: Electric field magnitude in the plane $y = 0.0$. Bottom: Electric field amplitude and field lines in the plane $z = 130.0$ mm at phase $\phi = 90.0^{\circ}$.

10 TE11 mode in a circular waveguide

Tutorial 9 showed that it is relatively easy to initiate a TE_{10} mode in a rectangular waveguide. Here, the drive current density has a simple cosine spatial dependence. In contrast, the ideal spatial variation of current density to drive a circular waveguide would be quite difficult to approximate with the expressions available in the algebraic parser. For reference, the transverse components of magnetic field of the TE_{11} mode in a circular waveguide of radius a vary is

$$H_r = H_0 \left[\frac{J_1(hr)}{hr} - J_2(hr)\right] \cos\phi, \tag{21}$$

$$H_\phi = -\frac{H_0}{hr} J_1(hr) \sin\phi, \tag{22}$$

where J_1 and J_2 are Bessel functions and $h = 1.841/a$. The corresponding current-density components can be expressed as:

$$r = \sqrt{x^2 + y^2}, \tag{23}$$

$$j_x(x,y) = \frac{2H_0}{\Delta} \left(\frac{x}{r}\right)\left(\frac{y}{r}\right) J_2(hr), \tag{24}$$

$$j_y(x,y) = \frac{2H_0}{\Delta} \left[\frac{J_1(hr)}{hr} - J_2(hr)\left(\frac{x}{r}\right)^2\right]. \tag{25}$$

where Δ is the layer thickness. In practical cases, we need not worry about replicating this variation exactly. Generally, a circular waveguide is operated in a frequency range where the TE_{11} mode is the only one that can propagate. If all other modes are evanescent, we can be certain that only the TE_{11} mode will propagate downstream, even if the current density is a rough approximation to Eqs. 24 and 25.

The example `TE11` illustrates the setup. The geometry consists of a metal waveguide of length 50.0 cm with $a = 5.0$ cm. Absorbing layers of thickness $\Delta = 0.25$ cm are located on the upstream and downstream ends. The cutoff frequency for the mode is

$$f_c = \frac{0.293c}{a}. \tag{26}$$

For the given dimensions, $f_c = 1.757$ GHz. The wave is driven by a uniform current density $j_x = 1.0$ A/cm^2 in the upstream absorbing layer.

In the first example (`TE11.AIN`), excitation at 2.5 GHz produces a traveling wave above cutoff. The wavelength in the guide is given by

$$\lambda_g = \lambda_0\sqrt{1 - (f_c/f)^2}). \tag{27}$$

where $\lambda_0 = c/f = 12.0$ cm. The guide wavelength is $\lambda_g = 16.88$ cm. From the discussion of Tutorial 9, the matched conductivity of the absorbing layer for a propagating waveguide mode is

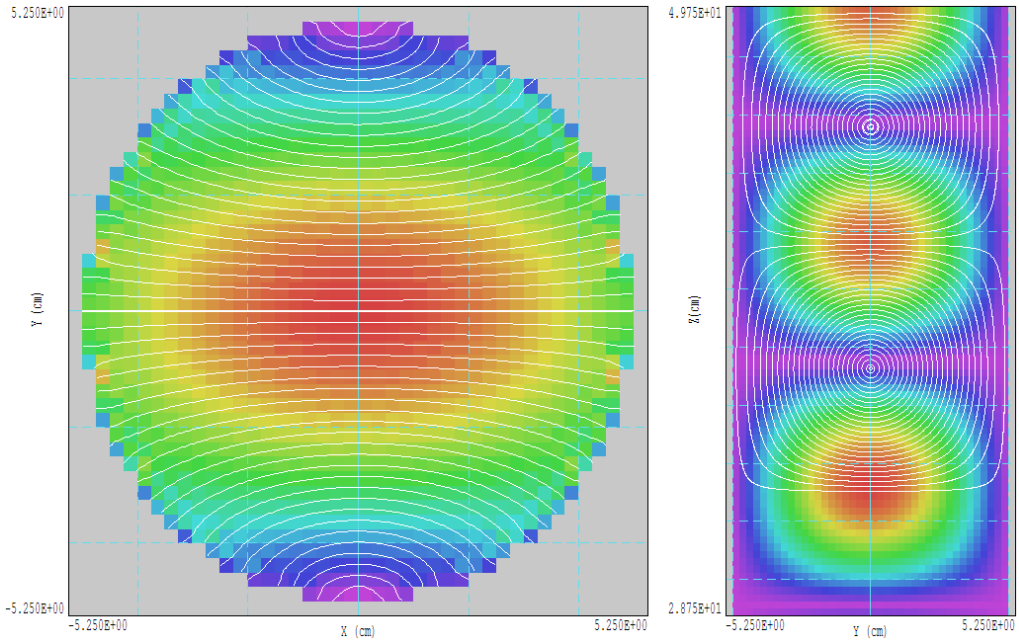

Figure 28: Propagating TE_11 mode in a circular wave, color coding shows $|\mathbf{E}|$ at a reference phase of 0.0°. Lines of electric field in a plane normal to z. Right: lines of magnetic field in a plane normal to x.

$$\sigma = \frac{1}{\eta_0 \Delta} \left(\frac{\lambda_0}{\lambda_g} \right), \tag{28}$$

where $\eta_0 = 376.7\ \Omega$. Inserting parameters in Eq. 28 gives the value $\sigma = 0.755$ S/m. Figure 28 shows electric and magnetic field lines of the propagating mode. A scan of $|\mathbf{E}|$ along z in the right-hand figure confirms that the guide wavelength equals the theoretical value.

In a second run (`TE11E.AIN`), the frequency is reduced to 1.6 GHz, a value below cutoff. Figure 29 shows the resulting distribution of $|\mathbf{E}|$ in the plane $x = 0.0$ cm. In this case, the field amplitude of the evandscent wave is predicted to vary as $\exp(-\gamma z)$, where

$$\gamma = h \sqrt{1 - \left(\frac{f}{f_c} \right)^2}. \tag{29}$$

For the given parameters, $\gamma = 15.20\ \mathrm{m}^{-1}$. The theoretical e-folding distance for reduction of the wave amplitude is 6.6 cm. For comparison, a line scan of $|\mathbf{E}|$ along the axis in Fig. 29 shows an exponential variation with 7.1 cm e-folding distance.

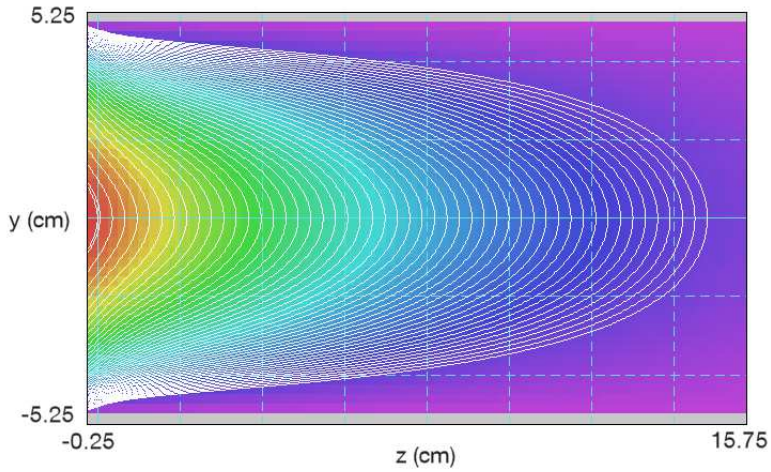

Figure 29: Evanescent wave in a circular waveguide, $|\mathbf{E}|$ in the plane $x = 0.0$ cm along with lines of $|\mathbf{H}|$. The source layer is on the left.

11 S matrix for a two-terminal network

This tutorial addresses two computational techniques: 1) finding the S (scattering) parameters of a microwave network and 2) extraction of traveling wave components from the complex field values generated by **Aether**. Suppose we have a multi-port network where a device connects identical waveguides (or transmission lines). We denote the waveguides as Port 1, Port 2,.... For simplicity, we shall neglect power absorption within the ports. At a given frequency the ports carry the same electromagnetic mode at locations far from the device. The relative mode amplitudes in different ports may be characterized by an electric field value (*e.g.*, electric field amplitude at a reference point, line integral of electric field amplitude,...). Suppose we excite Port 1 with an incident wave with electric-field amplitude E_{i1} and place matched terminations on the other ports. In this case, there is reflected wave in Port 1 (E_{r1}) and transmitted waves in the other ports (E_{t2}, E_{t3}, E_{t4},...). The coefficients in the first column of the S matrix are:

$$S_{11} = \frac{E_{r1}}{E_{i1}}, \quad S_{21} = \frac{E_{t2}}{E_{i1}}, \quad S_{31} = \frac{E_{t3}}{E_{i1}}, \ .... \tag{30}$$

There are several ways to find the ratios in Eq. 30 using **Aether**. To start, we need to know the electric field and power flux for an incident wave in the waveguide (or transmission line) corresponding to a given drive source current distribution. Sometimes, it is possible to find the values from analytic expressions. In the general case, we set up an **Aether** calculation for a short section of the line with a matched termination. Tutorial 2 illustrates the procedure for a transmission line and Tutorial 9 covers a rectangular waveguide. If we apply the current source at Port 1 of the network, then we know the quantities E_{i1} and P_{i1}. If we put matched terminations on the other ports, then we can find the transmitted field magnitude and power for excitation at Port 1. The off-diagonal S matrix parameters are given by

$$S_{21} = \frac{E_{T2}}{E_{I1}}, \quad S_{31} = \frac{E_{T3}}{E_{I1}}, \ ..., \tag{31}$$

or

$$S_{21} = \sqrt{\frac{P_{t2}}{P_{i1}}}, S_{31} = \sqrt{\frac{P_{t3}}{P_{i1}}}, ... \tag{32}$$

If the microwave device does not absorb or create energy, the diagonal element is given by

$$S_{11} = \sqrt{1 - \frac{P_{t2}}{P_{i1}} - \frac{P_{t3}}{P_{i1}} ....} \tag{33}$$

The component S_{11} may also be determined from the voltage standing-wave-ratio in Port 1. An axial scan of electric field amplitude at the reference position yields the maximum and minimum field values, E_{max} and E_{min}. The standing-wave ratio is

$$S_{wr} = \frac{E_{\max}}{E_{\min}} \ . \tag{34}$$

The scattering matrix component is given by

$$S_{11} = \frac{S_{wr} - 1}{S_{wr} + 1}. \tag{35}$$

Equations 34 and 34 may not be accurate for high reflection ratio, $S_{11} \cong 1.0$.

An alternative approach that does not require a preliminary solution is to find E_{i1}, E_{r1}, E_{t1}, E_{t2},... directly from the complex-number values generated by **Aether**. It is easy to find the transmitted field amplitudes (E_{t1}, E_{t2},...) because the fields in the terminated output ports are pure traveling waves. The challenge is to separate the mixed incident and reflected waves in the input port. The electric field of the incident wave has the axial variation $\exp(-jkz)$ where $k = 2\pi/\lambda$. Here, λ is the axial wavelength in the waveguide. The reflected wave varies axially $\exp(+jkz)$. Suppose we measure complex-number values of electric field at two positions in Port 1 far from the device: E_1 at z_1 and E_2 at z_2. We can express the values in terms of the traveling waves as

$$E_1 = E_i \ \exp(-jkz_1) + E_r \ \exp(jkz_1), \tag{36}$$
$$E_1 = E_i \ \exp(-jkz_2) + E_r \ \exp(jkz_2). \tag{37}$$

Inverting Eqs. 36 and 37 gives a relationship for E_r and E_i in terms of the measured quantities:

$$E_i = \frac{E_2 \ \exp(-jkz_2) - E_1 \ \exp(-jkz_1)}{\exp(-2jkz_2) - \exp(-2jkz_1)}, \tag{38}$$
$$E_r = \frac{E_2 \ \exp(jkz_2) - E_1 \ \exp(jkz_1)}{\exp(2jkz_2) - \exp(2jkz_1)}. \tag{39}$$

The measurements positions should not have a separation that gives a value of zero in the denominator: $\lambda/2$, λ, $3\lambda/2$, ...

The example `SMATRIX` illustrates the calculation for a two-port network. A rectangular vacuum waveguide carrying a TE_{10} mode at $f = 11.4$ GHz is interrupted by a rectangular iris. The waveguide has dimensions $a = 22.86$ mm and $b = 10.16$ mm. The cutoff frequency is $f_c = c/2a = 6.56$ GHz and the vacuum wavelength is $\lambda = c/f = 26.32$ mm. The guide wavelength is

$$\lambda_z = \frac{\lambda}{\sqrt{1 - (f_c/f)^2}} = 32.18 \text{ mm}, \tag{40}$$

and the wavenumber is $k = 2\pi/\lambda_z = 195.25$ m^{-1}. The aperture in the iris has dimensions $\Delta x = 11.00$ mm and $\Delta y = 5.00$. The iris thickness is 2.0 mm.

The file `SMATRIX.MIN` defines a solution volume that covers a 100 mm length of waveguide with the aperture at the midplane. There are upstream and downstream absorbing layers of thickness $\Delta z = 0.5$ mm. The upstream absorber carries a drive current to excite the TE_{10} mode with electric field in the y direction. As described in Tutorial 9, the matched conductivity of the absorbing layers is given by

$$\sigma = \frac{1}{\sqrt{\mu/\epsilon}\Delta z} \sqrt{1 - (\lambda/2a)^2}. \tag{41}$$

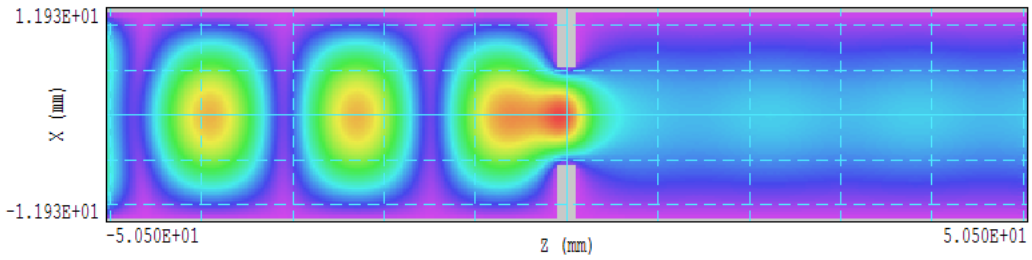

Figure 30: Electric field amplitude $|E_y|$ in the plane $y = 0.0$ mm.

For the parameters of the example, $\sigma = 4.3413$ S/m.

An initial **Aether** run (`SMATRIX_01.AIN`) was performed to characterize the incident wave. In this run, the physical properties of the elements representing the iris were set to those of air. The resulting wave was close to a pure traveling wave. There was a small component of standing wave ($S_wr \cong 1.07$) because of imperfect absorption on the end layers. The average electric-field amplitude of the traveling wave was $|E_y| = 1.47 \times 10^5$ V/m at $x = 0.0$ mm. The power absorbed in the downstream termination was 2.69 kW.

Figure 30 shows the amplitude of the electric field in the plane $y = 0.0$ with a metal iris. As expected, there is a strong standing wave upstream and a downstream traveling wave. The wave amplitude in the downstream region is approximately 1.02×10^5 V/m, implying that $S_{12} = 0.69$. The computed time-averaged power in the downstream absorber is 1.29 kW. The value predicted for S_{12} from Eq. 32 is also 0.69. A scan along the axis through Port 1 gives the maximum and minimum values of electric field amplitude, $E_max = 2.627 \times 10^5$ V/m and $E_min = 3.847 \times 10^4$ V/m. The standing wave ratio is $S_{wr} = 6.83$. Equation 35 gives a value $S_{11} = 0.74$. Conservation of energy implies that $S_{11}^2 + S_{21}^2 = 1.0$. Using the values from the calculation, $0.69^2 + 0.74^2 = 1.02$.

Finally, we can check the value of S_{11} by finding the ratio of reflected to incident wave in Port 1 using the *RI tool* in **Aerial**. To use the tool, you must first enter the value of the mode wavelength. Click on the *Set guide wavelength* command and enter $0\lambda = .03218$ m. Set up a slice plot normal to the y axis near $y = 0.0$ mm. Click on the *RI tool* and use the mouse to define two points at the same value of x separated in z by a distance of about $\lambda/4$. **Aerial** writes a summary of results to the screen and an entry like the following entry if a data record file is open:

```
Wave decomposition into incident and reflected parts
   Point 1
      X:   7.00005E-02
      Y:  -2.50000E-01
      Z:  -3.85000E+01
   Point 2
      X:   7.00005E-02
      Y:  -2.50000E-01
      Z:  -3.35000E+01
   EpsiR:   1.00000E+00
   MuR:   1.00000E+00
   Lambda:   3.21800E-02 (m)
   (z2-z1):  -3.35000E-02 (m)
```

```
(z2-z1)/Lambda: -1.0410
|ExI|:   6.95322E+01  |ExR|:   5.33534E+01
|EyI|:   1.50672E+05  |EyR|:   1.11892E+05
|EzI|:   4.53467E+03  |EzR|:   2.61847E+03
```

The ratio of reflected to incident wave is $|E_{yr}|/|E_{yi}| = 0.74$, in agreement with the other methods.

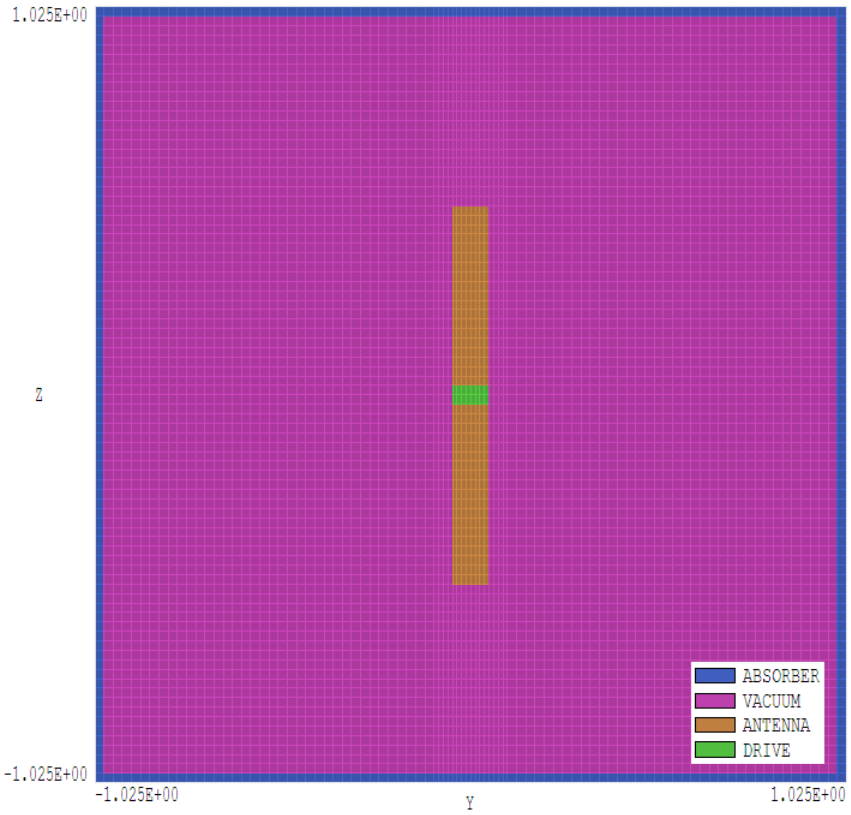

Figure 31: Geometry to model a half-wave dipole.

12 Half-wave dipole antenna

This tutorial demonstrates general techniques for frequency-domain models of metal antennas using **Aether**. The example also emphasizes precautions you should take in comparing results for detailed three-dimensional systems to ideal theoretical predictions. The files `HALFWAVE01.MIN` and `HALFWAVE01.AIN` describe a half-wave dipole. Figure 31 shows the geometry. The solution volume consists of a vacuum cube with sides of length 2.0 m surrounded by an absorbing layer of thickness 0.025 m. The antenna is a metal rod of radius $R = 0.05$ m and height $L = 1.0$ m. The condition $\lambda = 2L$ occurs at frequency $f = 1.5 \times 10^8$ Hz. A vacuum drive region of height 0.05 m at the center of the antenna carries a current with amplitude $I_m = 1.0$ A. With these parameters, an idea antenna should generate 36.54 W.

The **Aether** control script contains the following statements to define the drive current:

```
NPeriod = 6 2
SMod(1) = 0.0
Jz(4,1) = 123.1
```

The solution runs for six RF periods with a smooth start over two periods. The drive current density in the z direction has zero phase and a steady-state amplitude of $j_z = 123.1$. The

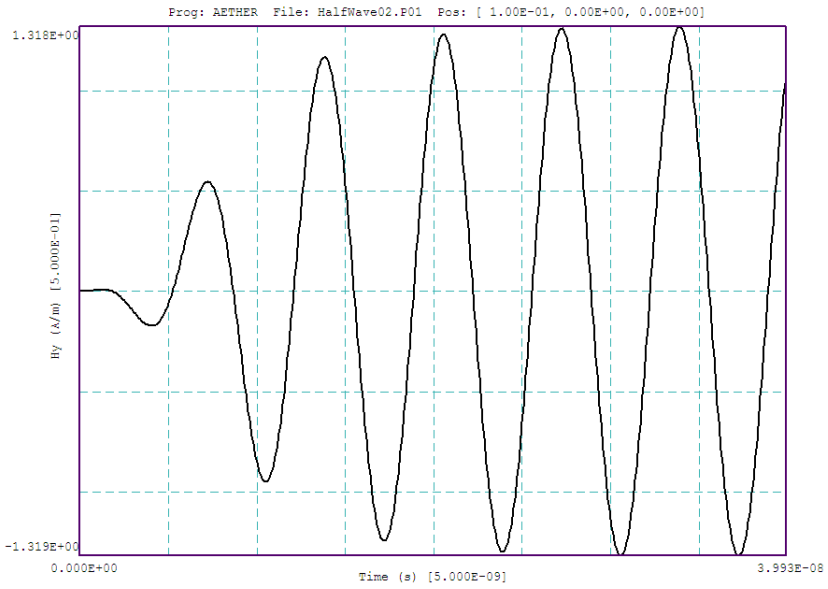

Figure 32:

current density equals 1.0 A divided by the cross section area of the drive region (52 elements with dimension 0.0125 m $\times$ 0.125 m). The bulk of the antenna is set as a metal region. A probe placed in the plane of peak radiation ($z = 0.0$ m) about halfway to the wall checks E_z. History monitors were placed at this position and also a $r = 0.10$ m to monitor the near fields.

The history record of H_y at $r = 0.5$ m, shown in Fig. 32, confirms that the highly-damped system reached equilibrium at $t = 6\tau$. After conversion to phasor form, **Aether** makes the following entry in the listing file:

```
Energy and power integrals
Global quantities
   Electric field energy:   1.88269E-07 (J)
   Magnetic field energy:   1.88766E-07 (J)
   Total field energy:   3.77035E-07 (J)
   Resistive power dissipation:   6.37745E+01 (W)
Region quantities
    NReg  ElecEnergy   MagEnergy    TotEnergy      Power
              (J)          (J)          (J)          (W)
   ============================================================
      1  2.65911E-09  8.11792E-10  3.47090E-09  6.37745E+01
      2  1.79649E-07  1.87305E-07  3.66953E-07  0.00000E+00
      3  0.00000E+00  0.00000E+00  0.00000E+00  0.00000E+00
      4  5.96118E-09  6.49320E-10  6.61050E-09  0.00000E+00
```

The solution agrees with predictions for the half-wave dipole in every respect except that the power of 63.77 W is almost is twice the prediction for an ideal antenna.

The difference follows from a non-intuitive characteristic of numerical electromagnetic simulations: it is relatively easy to represent real-world systems, but quite difficult to replicate ideal systems. In this case, we must recognize that the system as defined is not an ideal deal half-wave dipole. The center section has reactive elements that modify the impedance seen by

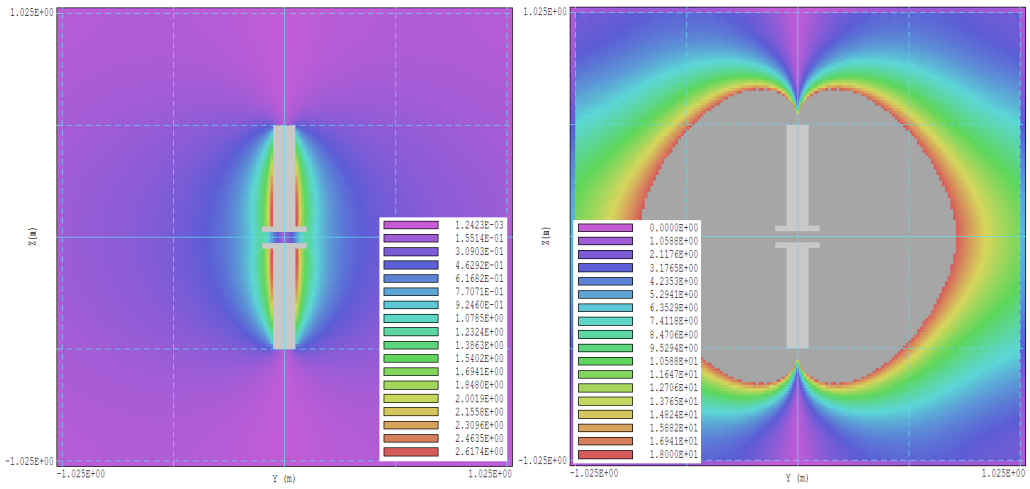

Figure 33: Half-wave dipole with capacitive loading at the drive gap. Left: $|\mathbf{H}|$ near the antenna. Right: $|\mathbf{S}|$ in the radiative region.

the drive current. As in the case of an actual antenna, matching components are required when connecting a 75 Ω line. There are two indications of mismatch: 1) the electric field in the gap is not exactly 180° out of phase with the drive current and 2) the value of H_y at the near-field monitor implies that the total gap current exceeds the drive current.

A change in the drive gap geometry significantly alters matching to the antenna (`HALFWAVE02.MIN`, `HALFWAVE02.AIN`). In the system of Figure 33, the radius of the drive region was expanded to 0.10 by adding caps. This change reduced the inductance and increased the capacitance of the gap. The drive current density was adjusted to 30.77 A/m^2 to maintain 1.0 A total. In this case, the radiated power dropped to 41.85 W. The phase of the electric field in the gap was 149.2°. The left-hand side of Fig. 33 shows the variation of H_y near the antenna. As expected, the magnitude of the drive current scaled as $\cos(\pi z/L)$. The right-hand side, which shows the amplitude the Poynting vector, illustrates the directionality of the radiated power.

In conclusion, when faced with mysterious results remember this general rule. **Aether** simulates what it sees, not necessarily what you want.

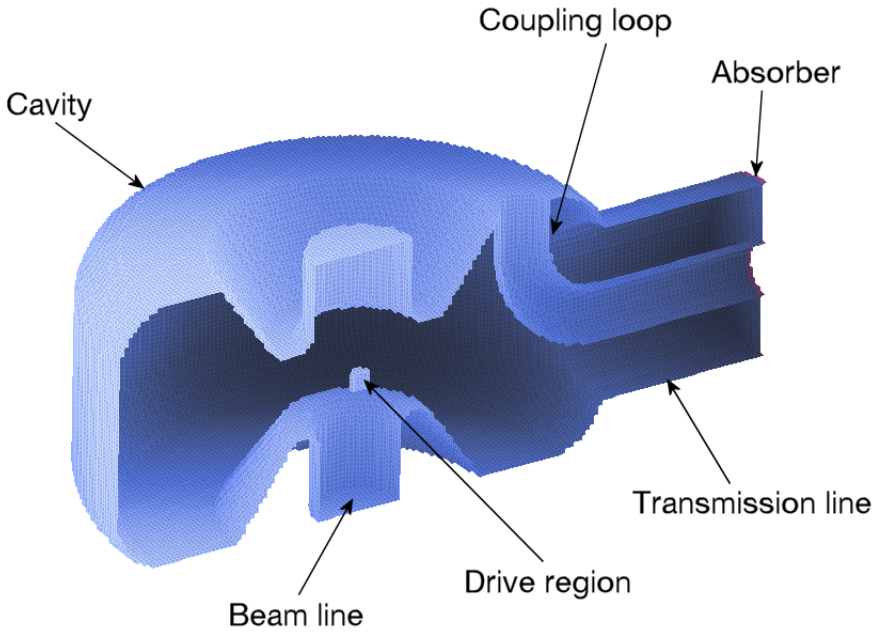

Figure 34: Cut-away view of a klystron output cavity coupled to a 75 Ω coaxial transmission line.

13 Loaded klystron output cavity

In contrast to the benchmark examples in this manual, this chapter discusses a significant design study using the full three-dimensional resources of **Aether**. The calculation addresses loading of the output cavity of a hollow-beam klystron. It is part of a larger study to optimize the coupling loop to an output transmission line to achieve a target value of loaded Q. For a discussion of the physics of klystrons, see S. Humphries, **Charged Particle Beams** (Wiley-Interscience, New York, 1990), Sects. 15.2, 15.3 and 15.4. The text is available for download at `http://www.fieldp.com/cpb.html`.

Figure 34 shows the simulation geometry, a reentrant output cavity for a high-power klystron. The cavity has an outer radius of 6.0 cm. The RF power is extracted through a 75 Ω vacuum coaxial transmission line with outer radius $R_o = 2.0$ cm and inner radius $R_i = 0.6$ cm. For the study it is assumed that there is an ideal vacuum window at a downstream point in the line so that there is no reflected power. The calculation represents a 4.0 cm length of the line with an absorbing boundary layer at the end. There are three primary quantities to find: 1) the resonant frequency of the structure, 2) the peak electric field levels and 3) the Q factor determined by output loading.

13.1 Resonant frequency calculation

The first task was to find the resonant frequency of the loaded cavity. To check the 3D model, a 2D calculation was performed for a cylindrically-symmetric cavity without the transmission

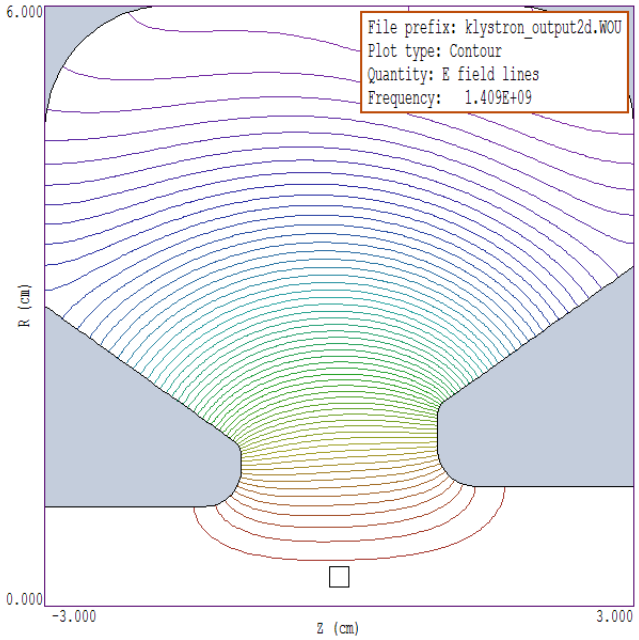

Figure 35: Cavity geometry and electric field lines. Two-dimensional **WaveSim** calculation.

line. The files `KLYS_FREQ2D.MIN` and `KLYS_FREQ2D.WIN` were input to **Mesh** and **WaveSim** of the **TriComp** series. The test was definitive because **WaveSim** used completely different numerical methods: triangular elements and a solution of the Helmholtz equation by a direct matrix inversion. Figure 35 shows a z-r plot of the cavity geometry and electric field lines of the fundamental mode. The beam transport line was below cutoff; therefore, the boundaries at $z = \pm 3.0$ cm did not affect the calculation. With an element size of 0.05 cm, the calculated TM_{010} frequency was 1.409 GHz.

The vectors comprising the outline of the cavity wall (`KLYSTRON.OTL`) were transferred to the **MetaMesh** file `KLYS_FREQ3D_NL.MIN` to generate a three-dimensional representation with an element size of 0.1 cm. The mesh had 627,669 elements. The strategy in **MetaMesh** was to fill the solution volume with metal elements and then to carve out the cavity using the outline created in the **Mesh** drawing editor. The resonator simulations involved a large number of metal elements, but there was no time penalty because **Aether** does not update field values inside metal regions. A small region with a drive current density j_z was located on axis (Fig. 34) to limit the response to modes of type TM_{010}. With excitation in the frequency band 0.0 to 3.0 GHz, **Aether** detected a single resonance at 1.402 GHz, within 0.5% of the **WaveSim** result. The calculation took one hour on a 2.83 GHz dual-core computer.

The next step was to find the resonant frequency of the full system with the terminated transmission line. Table 9 shows the contents of the **Aether** script `KLYS_FREQ3D.AIN`. The *Source* command defined a uniform current in the z direction in the drive region (Region 4). Region 1 comprised the cavity wall and the inner and outer conductors of the transmission line. Region 2 was the cavity volume and Region 3 was the line terminator (with thickness 0.1 cm). A probe was located at radius 5.50 cm across from the coupler. Figure 36 shows the Fourier transform of the probe signal near the resonance. The inclusion of the transmission line coupler reduced the cavity volume and consequently shifted the frequency up about 0.9% to 1.4209 GHz. The width of the response gave a rough estimate of the quality factor, $Q \sim 24.5$.

Table 9: Contents of the file KLYS_FREQ3D.AIN.

```
* ---- CONTROL ----
Mode = RES
Mesh = KLYS_FREQ3D
DUnit =  100.0
Freq 1.5E9 3.0E9
Source 4 0.0 0.0 1.0
* ---- REGION PROPERTIES ----
Metal(1)
Vacuum(2)
AbsLayer(3) 0.10
Vacuum(4)
* ---- DIAGNOSTICS ----
Probe =  -5.50 0.00 0.00  Hy
EndFile
```

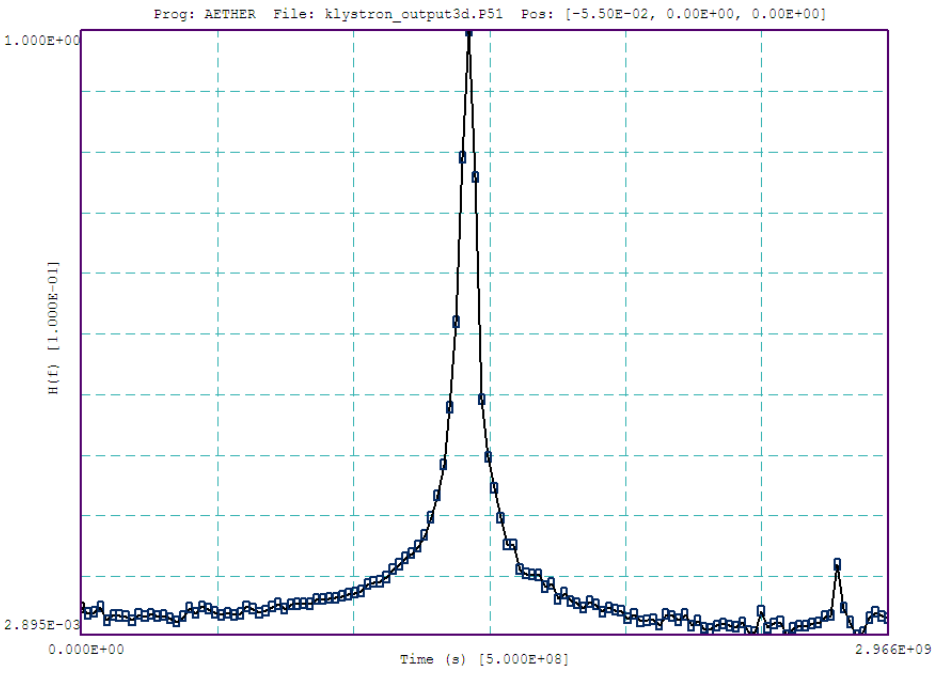

Figure 36: Frequency response of the loaded klystron cavity.

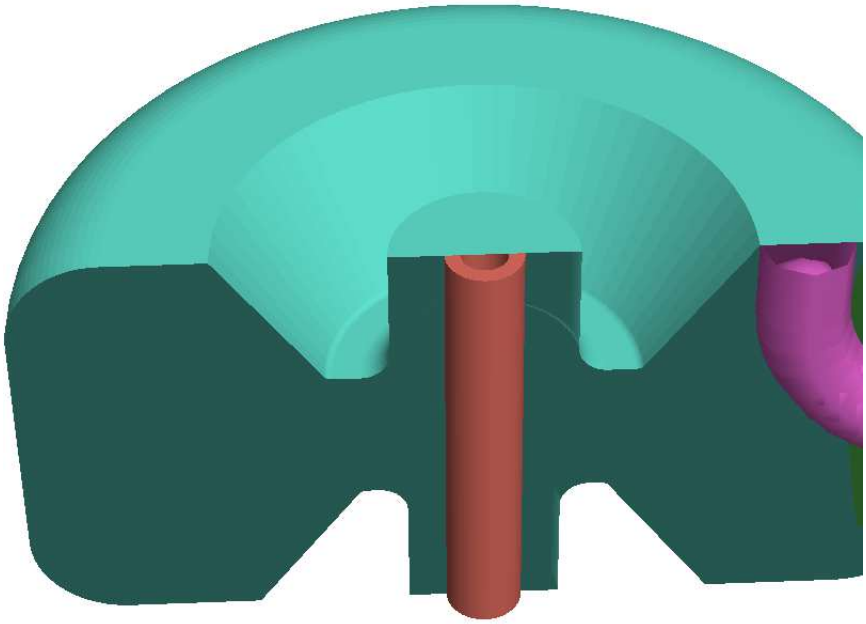

Figure 37: Annular beam drive current (orange) for the RF field solution.

13.2 Mode field calculation

The resonant frequency $f_0 = 1.4209$ GHz was used in the final RF-mode calculation to find the field distribution and an accurate value of Q for the driven cavity. The **Aether** script `KLYS_FIELD.AIN` contained the following lines:

```
Freq = 1.4209E9
NPeriod = 40 2
```

The relatively large number of RF periods was necessary to ensure that the fields reached equilibrium before conversion to phasor form. Some care must be taken to represent drive currents in a loaded RF solution. In this case, the drive was an annular beam with outer radius 0.5 cm and inner radius 0.3 that extended along the length of the transport tube. Figure 37 shows the mesh defined by `KLYS_FIELD.MIN`. The harmonic component of current at frequency f_0 in the bunched beam had amplitude $I_0 = 100$ A. The discrete representation of the beam cross-section included 48 elements, each with area 10^{-6} m^2. The current density to generate 100 A was $j_z = 2.083 \times 10^6$ A/m^2.

Figure 38 shows a plot of $H_y(t)$ at the probe position, confirming that the solution had reached a steady state. The run time was 1 hour and 20 minutes. One method to calculate cavity loading is to use the energy and power integrals recorded in the listing file. The quality factor is given by

$$Q = \frac{2\pi f_0 U}{P}, \tag{42}$$

where U and P are time-averaged values of the electromagnetic energy in the cavity and power dissipated in the absorbing layer. The values determined in the **Aether** solution were $U =$

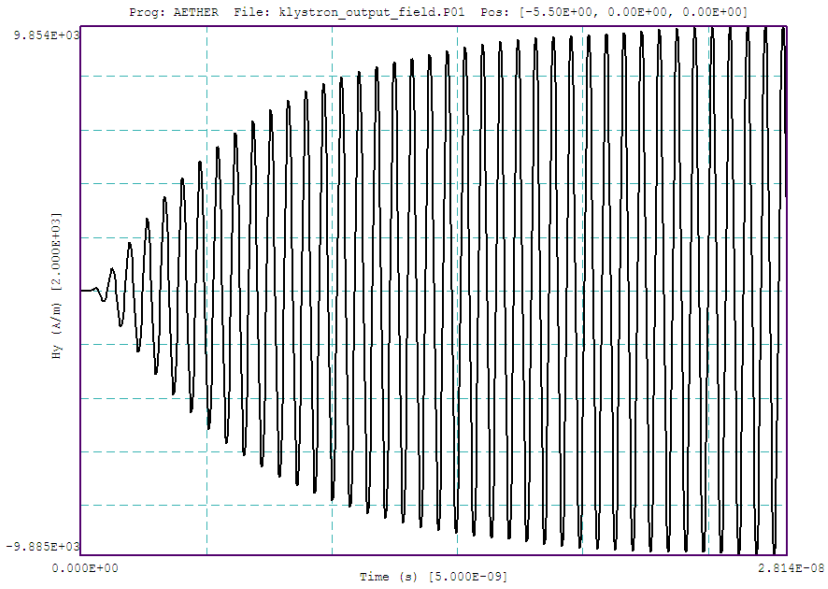

Figure 38: Plot of $H_y(t)$, monitor at a radius $r = 5.5$

0.0485 J and $P = 14.53$ MW. Substitution in Eq. 42 yields $Q = 29.8$. The Q value can also be determined from the signal envelope in Fig. 38. The theoretical variation is

$$H_y(t) = H_y(\infty) \left[1 - \exp\left(-\frac{\pi f_0 t}{Q}\right)\right]. \tag{43}$$

Measurements of the signal using **Probe** imply that $Q \cong 31.5$.

The final activity is to inspect the mode fields. Figure 39 shows the variation of $|\mathbf{E}|$ over the x-y plane at $z = 0.0$. Here, the amplitude symbol refers to the peak value in time of the sum of the spatial components of the electric field. Note that the uniform value in the transmission line indicates a wave traveling to the right in the transmission line with no reflection at the absorbing layer (VSWR = 0). Using the *Line integral* command in **Aerial**, the voltage in the transmission line was determined to be $V_L = 45.2$ kV at a phase of 240°. The corresponding power flux is

$$P = \frac{V_L^2}{2Z_0} = 13.62 \text{ MW}. \tag{44}$$

The peak electric field value in the solution of 2.26 MV/m occurred on the tip of the smaller nose. A line integral $\int \mathbf{E} \cdot \mathbf{dl}$ across the axis of the cavity gave a cavity voltage $V_c = 295.4$ kV at 180°. The predicted beam power is $P = I_0 V_c/2 = 14.8$ MW. Within the accuracy of the line integrals, the three methods for estimating the RF power are consistent.

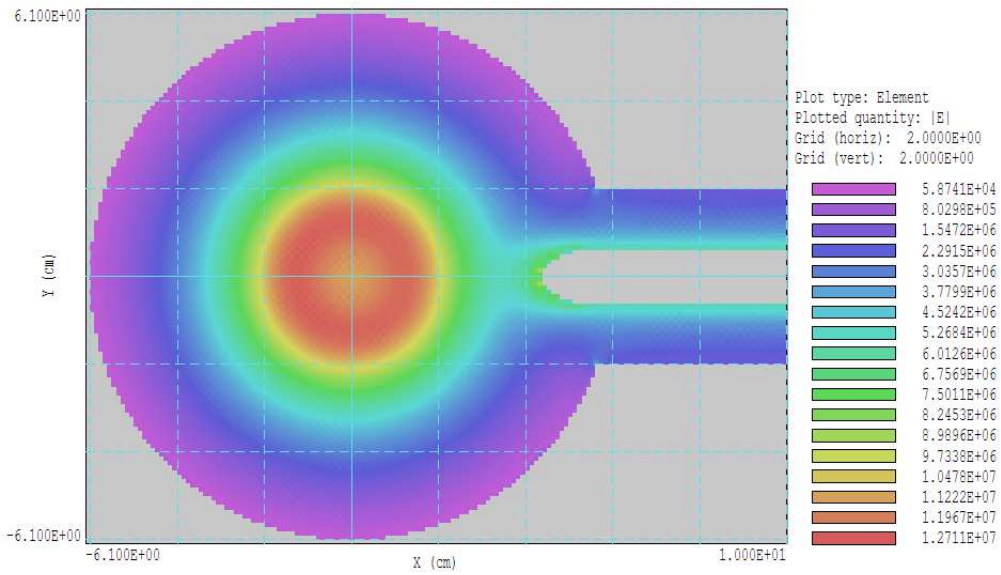

Figure 39: Variation of $|\mathbf{E}|$ in the plane $z = 0.0$ cm.

14 RF models of a cavity magnetron

The cavity magnetron is a widely-used source of high-power microwaves, from World War II radar to almost all microwave ovens. In this tutorial, I'll discuss the use of the 3D electromagnetic code **Aether** to find the resonant frequencies of a magnetron and to demonstrate the use of end-strapping to limit operation to a desired mode. Figure 40 illustrates the geometry. It shows a portion of the cross section of an eight-cavity structure, an extrusion of height H. We will associate the extrusion direction (out of the page) with the z axis of a three dimensional coordinate system. Electrons are emitted from a high-voltage cathode (A) and are pulled across the interaction region (B). Because of an applied axial magnetic field, the electrons cannot directly cross the gap but drift in the azimuthal direction. Cutouts in the grounded outer copper block define resonant cavities. The re-entrant shape of the cavities allows them to support a moderate frequency oscillation in a small structure. In the lowest order mode of a single cavity, an oscillating electric field drives current across the narrow gap (C). The current completes the circuit by flowing around the outer wall of the cylindrical chamber creating a magnetic field H_z. The gap (C) acts as a capacitor and the chamber (D) acts as an inductor, creating a resonant circuit. The azimuthal electric fields extend into the interaction region, influencing the drifting electrons so that they strike inner portions of the block in phase to yield energy to the oscillation. The self-consistent electron motion is a complex collective problem that must be approached with a particle-in-cell simulation. Here, I will address only the RF portion of the calculation.

I will pick a specific geometry, but build it in a way that would allow easy changes for other systems. The height of the block is $H = 8.0$ cm. A symmetry boundary in the middle can be applied to reduce the calculation time. In this case, the block extends from 0.0 to 4.0 cm in z. The eight inductive cutouts are cylinders of radius $R = 1.0$ cm with center displaced

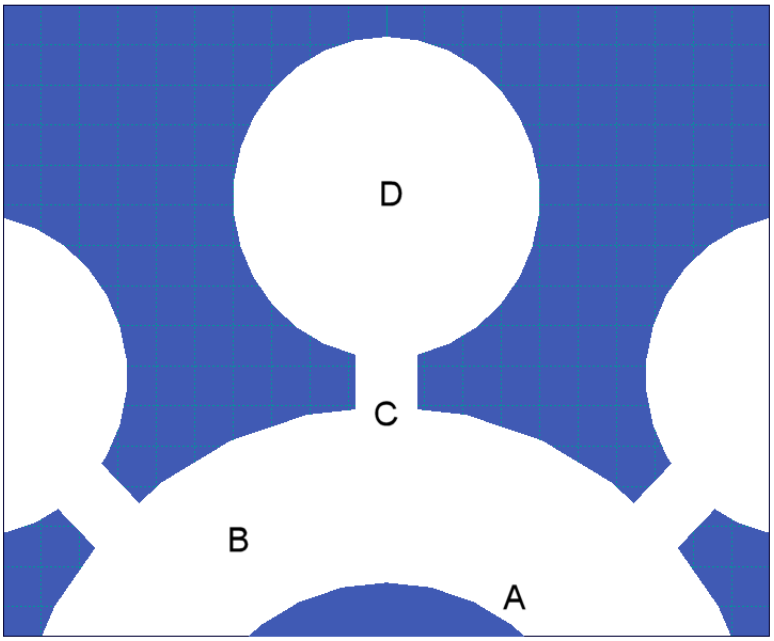

Figure 40: Cross-section of a cavity magnetron with eight cavities (detail)

3.8 cm from the axis. The capacitive slots have gap width $D = 0.4$ cm and length $L \approx 0.35$ cm. The interaction region has inner radius 1.4 cm and outer radius 2.5 cm. To set a starting point of the RF calculation, I made an estimate of the resonant frequency of a single cavity approximating fields as uniform in z. The capacitance of the gap is about

$$C \cong \epsilon_0 \frac{(2L)H}{D}. \tag{45}$$

The value 2 is a fudge factor to account for the energy of fringe fields around the narrow gap. Approximating the cylindrical chamber as a solenoid, the inductance is about

$$L \cong \mu_0 \frac{\pi R^2}{H}. \tag{46}$$

The single-cavity resonant frequency is

$$f = \frac{1}{2\pi\sqrt{LC}} \cong \frac{1}{2\pi\sqrt{\mu_0\epsilon_0\pi R^2(2L)/D}} \tag{47}$$

independent of the block height H. Inserting values for the test geometry, the frequency is $f_0 \cong 2$ GHz.

The cavities do not act independently, but are part of a periodic coupled structure. The RF oscillations are connected by shared electric fields in the interaction regions and shared magnetic fields at the top and bottom of the block. The coupled resonances would be difficult (if not impossible) to describe analytically, so a numerical calculation is required. Modes in a coupled structure are characterized by the oscillation phase differences in the individual components.

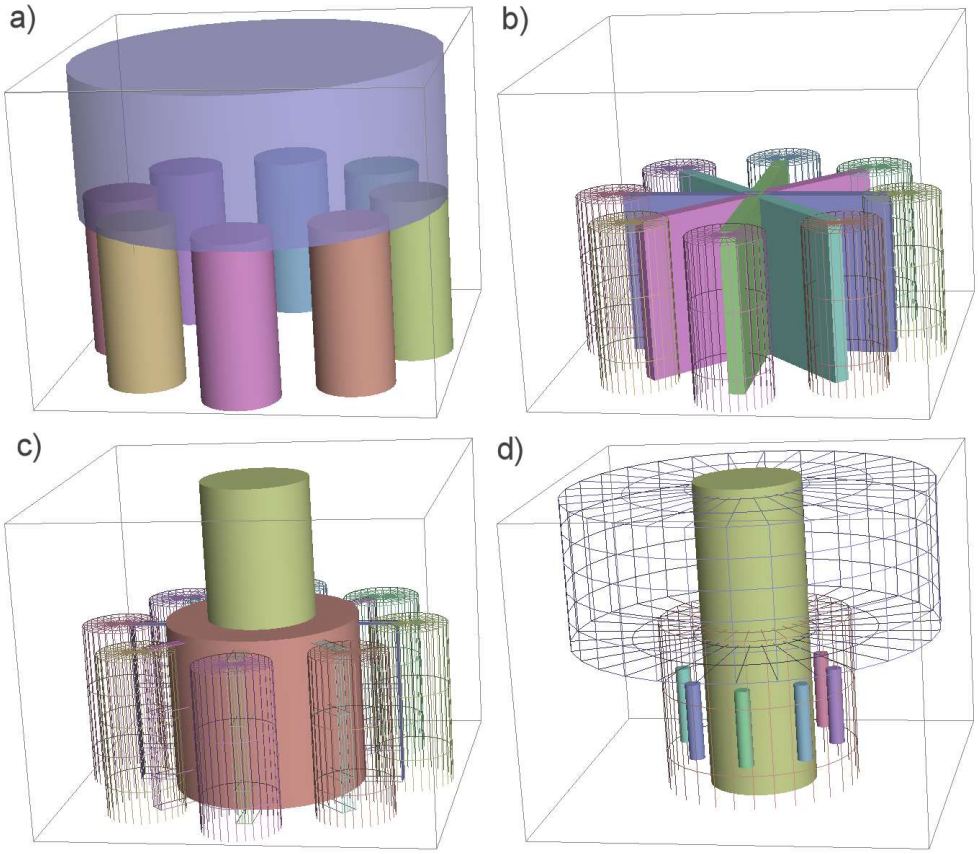

Figure 41: Steps in the construction of the mesh with **Geometer**.

The constraint is that the field quantities must repeat after eight components. We can express the axial magnetic field in the inductive region as

$$H_z = \cos(n\Delta\phi), \qquad n = 0, 7 \tag{48}$$

with the periodicity condition $1 = \cos(8\Delta\phi)$. The allowed values are

$$\Delta\phi = 0,\ \pi/4,\ \pi/2,\ 3\pi/4,\ \pi. \tag{49}$$

The value $\Delta\phi = \pi$ gives the strongest electron interaction and the highest efficiency, so the goal is ensure that the system operates in that mode.

The geometry is fairly complex, so I will summarize the steps in building the mesh using the **Geometer** and **MetaMesh** components of the **Aether** suite. Although I used a symmetry boundary at the midplane in z, I represented the complete system in the x-y plane to allow multiple models and to investigate the effect of end straps. Figure 41 shows the steps in creating the mesh specification. There were two main regions of material: vacuum and copper. All copper parts were set to ground potential because the static voltage between the cathode and anode does not affect the RF solution. The solution volume covered the region -5.0 cm $\leq x, y \leq$ 5.0 cm and 0.0 cm $\leq z \leq$ 8.0 cm. The first part to add was a box with the properties of copper that filled the entire solution volume (the outline in Fig. 41a). The next step was to define the top of the block and the end space by adding a cylinder of radius 4.0 cm and length

3.8 cm (blue) with the material properties of vacuum. The shape over-wrote the previous material property of copper for the included elements. In the default position, the cylinder extended between $z = \pm 1.9$ cm. After a shift $\Delta z = 5.9$ cm, the part extended between 4.0 cm $\leq z \leq$ 7.6 cm, defining a closed void above the block. The first cavity was a cylinder with vacuum properties of radius 1.0 cm and length 8.0 cm displaced 3.8 cm in x. The portion of the cylinder outside the solution volume was ignored by the codes. The other seven cavities were identical, except with different x-y shifts (in 45°increments). The operation could be performed within **Geometer** by duplicating the part and editing its shifts. Alternatively, the original part could be copied and pasted in the **MetaMesh** input script with the shifts modified with a text editor.

The next step (Fig. 41b) was to add the connecting slots to the interaction regions. The first slot (blue) was a box with dimensions $L_x = 7.0$ cm, $L_y = 0.4$ cm and $L_z = 8.4$ cm. It overlapped a small distance into the first and fifth cavities and extended across the central region. Two more such shapes were added with rotations of 45°and 90°as shown. The next step (Fig. 41c) was to carve out the interaction region, a cylinder of radius 2.5 and length 8.0 cm with vacuum properties. I then added the cathode, a cylinder of radius 1.4 cm with copper properties that extended the length of the solution volume. The mesh was completed by adding small cylinders with the material properties of vacuum that would carry drive currents to excite the RF oscillation in **Aether** (Fig. 41d). Each source had its own region number to allow assignment of specific current directions. The sources were cylinders with radius 0.2 cm and length 2.0 cm. They were shifted 2.0 cm in z, with x and y shifts to place them at a radius of 2.0 cm at 45°intervals.

Figure 42 shows the mesh generated by **MetaMesh** from the input specifications. With an element resolution of 0.1 cm, the mesh contained 800,000 elements. The procedure described used the basic combinatorial solid geometry capability of **Geometer** and **MetaMesh**. Alternatively, the programs could accept geometric information from 3D CAD programs in the form of STL files. The main advantage of the solid geometry approach is that it generates a parametric model of the geometry that is accessible to the user as a text file. For example, one entry for a part in the file appears as

```
PART
  Region: AIR
  Name: CAVITY1
  Type: Cylinder
  Fab:   1.00000E+00  8.40000E+00
  Shift:   3.80000E+00  0.00000E+00  0.00000E+00
END
```

The data could be copied, pasted and modified in a text editor to create multiple cavities. Find and replace operations could be used to make quick global changes to the geometry. Optionally, **MetaMesh** could be called as a background **Windows** task with properties specified as pass parameters in a batch file. In this way, a range of geometries could be investigated automatically.

With the mesh completed, I turned to the RF calculations using the resonance and RF modes of **Aether**. The first step was a resonance search over broad frequency range centered near $f_0 = 2.0$ GHz. To emphasize the π mode, I assigned azimuthal current density to the eight source regions, alternating counter-clockwise and clockwise. The copper region was defined as metal ($\epsilon_r = 10^6,\ \mu_r = 10^{-6}$) and all other regions had the property of vacuum ($\epsilon_r = 1,\ \mu_r = 1$).

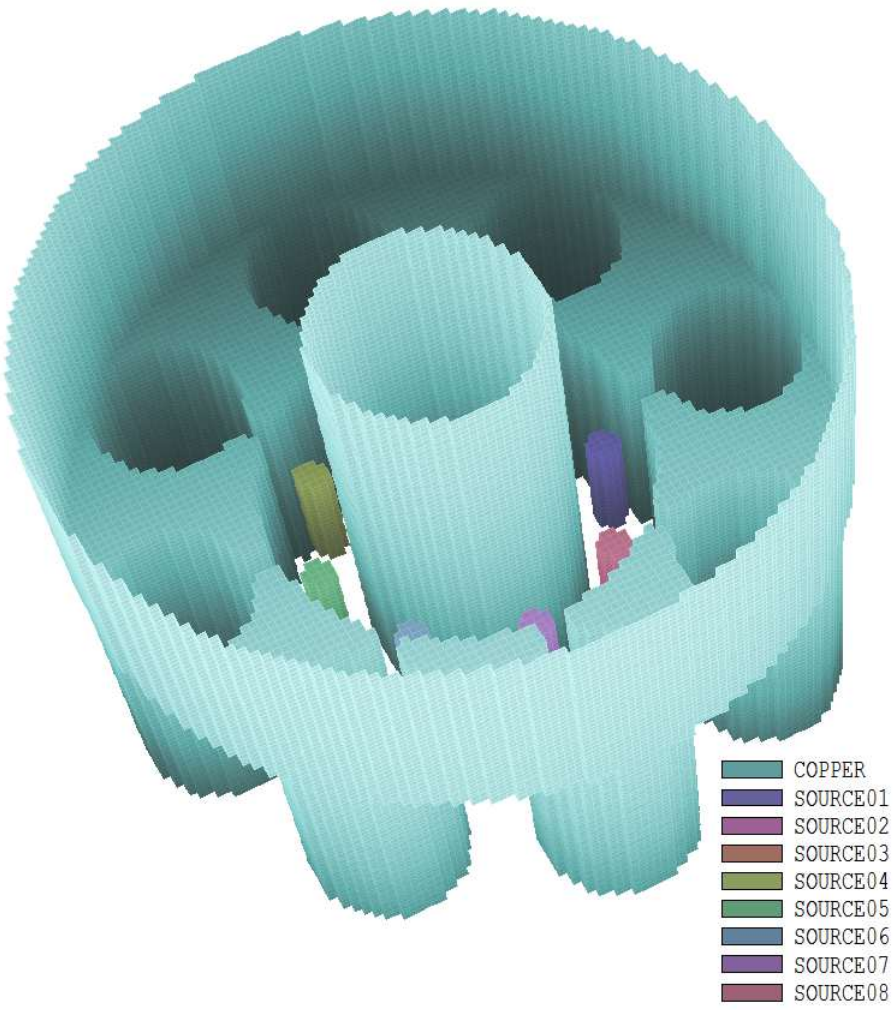

Figure 42: Completed mesh with the end plate at top removed.

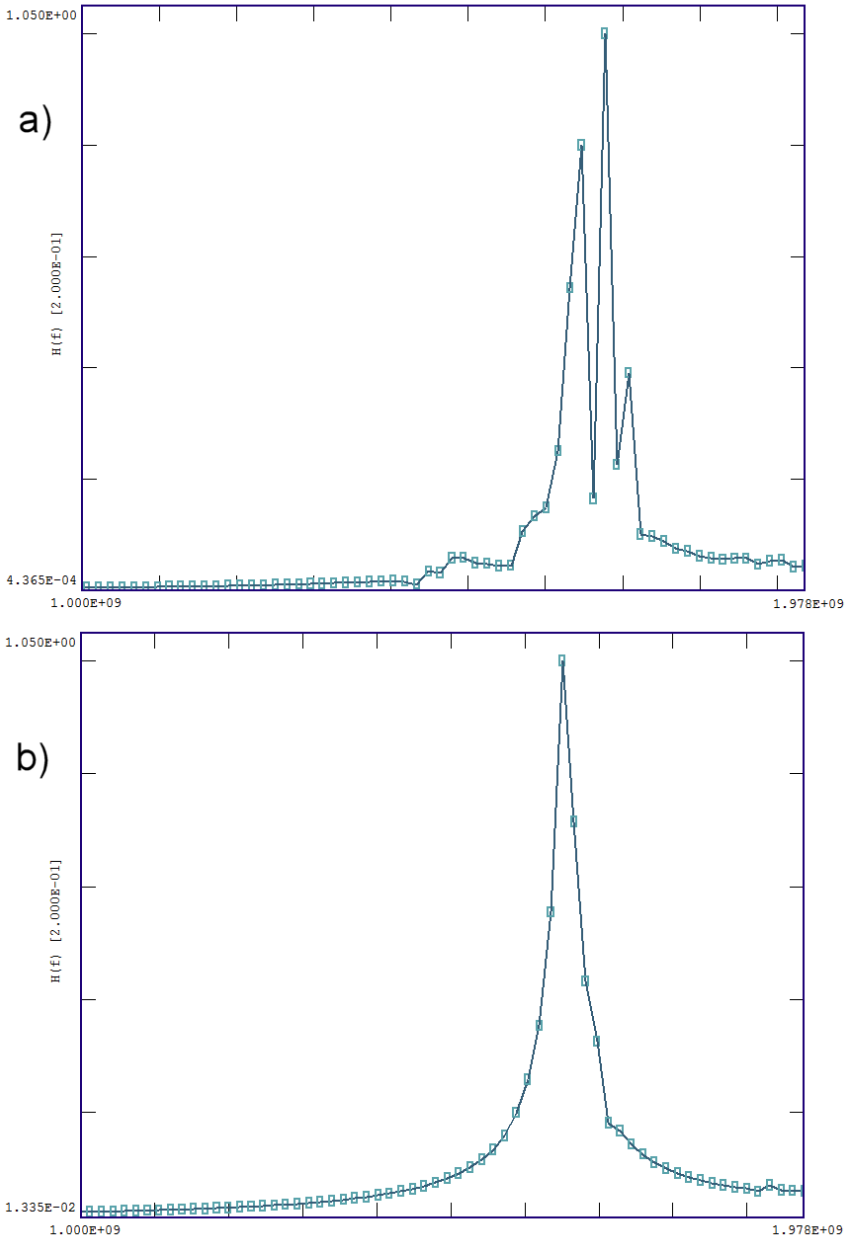

Figure 43: Frequency spectra for a resonance mode calculation. a) No strapping. b) With strapping.

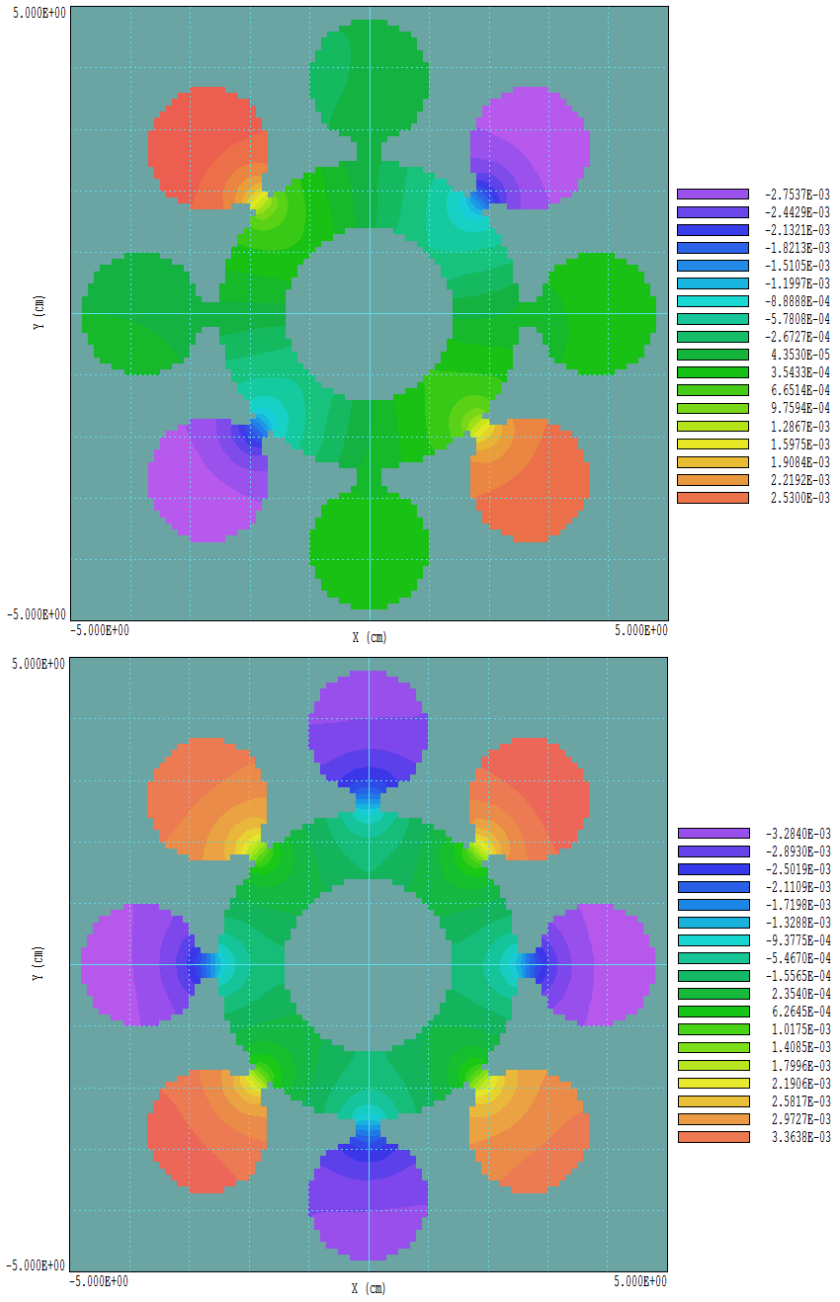

Figure 44: Plots of H_z in the plane $z = 2.0$ cm at a reference phase $\phi = 20^o$. a) $f_0 = 1.653$ GHz, no strapping. b) $f_0 = 1.652$ GHz, with strapping.

In the resonant mode, **Aether** excites a time-domain solution by driving the sources with a pulse whose Fourier transform is a rounded step function with a specified central frequency and frequency width. I set the code to monitor the variation of H_z in the first cavity over several RF periods. At the end of the run, the code takes a Fourier transform of the probe signal. The initial run showed activity near 1.7 GHz. I then made a detailed run with $f_0 = 1.7$ GHz and $\Delta f = 0.5$ Ghz. A narrow frequency band requires an extended run time. With 4-core parallel processing, the calculation ran about 17 minutes. The run yielded the plot of Fig. 43a which clearly shows the presence of multiple modes. The program also provides a detailed analysis of the probe signal using a peak-fitting routine. The three peaks corresponded to frequencies 1.653 GHz, 1.673 GHz and 1.692 GHz.

Next, I set up **Aether** solutions in the RF mode to associate the frequencies with modes. In this mode, the program determines a frequency-domain solution by running a time-domain solution to equilibrium and then converting the field values to phasor form. The waveforms for drive currents are time-modulated harmonic functions at a single frequency. Calculations in the RF mode run quickly, in this case about 2-3 minutes. The calculation at $f_0 = 1.653$ GHz gave the result shown in Fig. 44a. The figure, a cross-section in a plane normal to the axis, plots H_z at an axial position near the block center at a reference phase of 20°. The color coding indicates almost a pure $\Delta\phi = \pi/2$ mode. A similar plot for $f_0 = 1.692$ corresponded to the $\Delta\phi = \pi$ mode. In this case there were significant variations of field amplitude between cavities, indicating the presence of other modes.

The process of strapping is used in magnetrons to encourage the preferential excitation of the $\Delta\phi = \pi$ mode. The idea is to add structures at the ends of the block that enhance inductive and capacitive coupling between the resonant cavities. Figure 45 shows the modified mesh geometry with a single-ring end strap. The circular strap was connected to only odd-numbered segments of the block. This connection method reduced the frequency of the pi mode and raised that of the other modes. With increased frequency separation, I expected that the alternating azimuthal currents of the sources will excite only the $\Delta\phi = \pi$ mode. Figure 43b shows the results of a resonant mode calculation with the modified geometry. There was a single resonance at 1.652 GHz with very little additional activity. A run in the RF mode at this frequency yielded the result of Fig.44b. The values of $|H_z|$ were almost identical in all cavities, indicating a pure $\Delta\phi = \pi$ excitation.

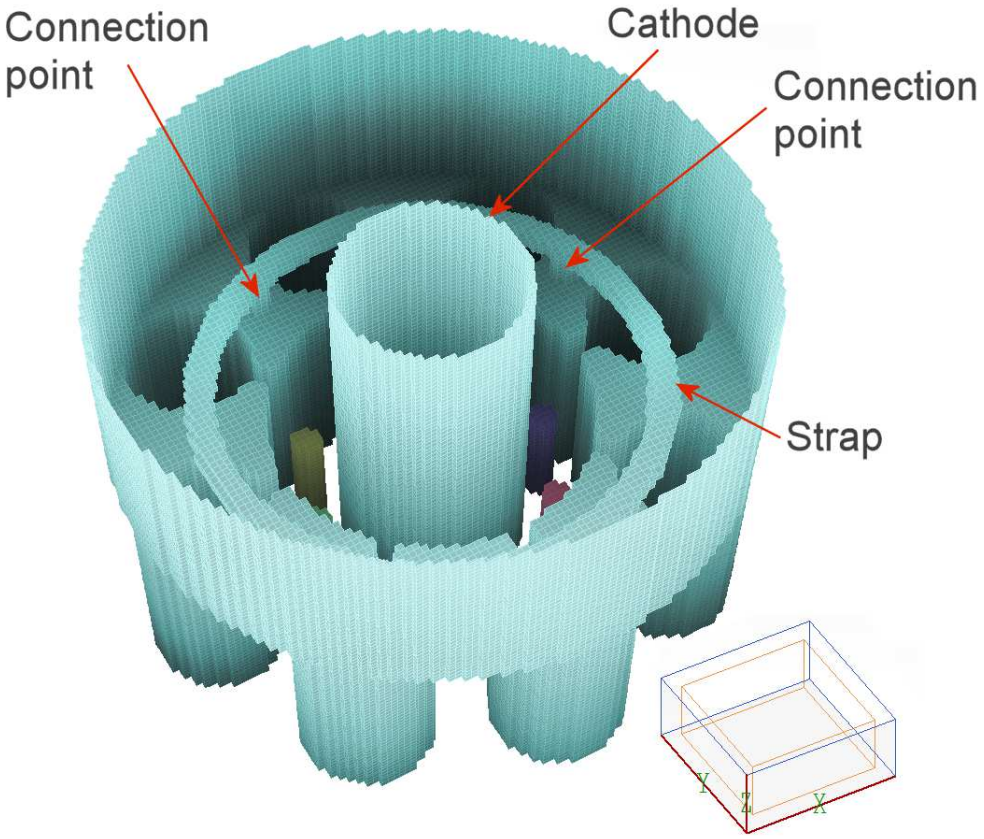

Figure 45: Single ring end strap added to the mesh.